UNIVERSITY OF CALIFORNIA

Santa Barbara

Interactions of a Paracyclophane-based Conjugated Oligoelectrolyte with Biological Membranes

A Thesis submitted in partial satisfaction of the

requirements for the degree Master of Science

in Chemistry

by

Jakkarin Limwongyut

Committee in charge:

Professor Guillermo C. Bazan, Chair

Professor Javier Read de Alaniz

Professor Frederick W. Dahlquist

Professor Kevin W. Plaxco

March 2019

The thesis of Jakkarin Limwongyut is approved.

_____
Javier Read de Alaniz

_____
Frederick W. Dahlquist

_____
Kevin W. Plaxco

_____
Guillermo C. Bazan, Committee Chair

March 2019

Interactions of a Paracyclophane-based Conjugated Oligoelectrolyte with Biological Membranes

Acknowledgements

I would like to begin this section by acknowledging Professor Guillermo C. Bazan for the opportunity to work under his supervision with well-equipped laboratories and instruments. I truly appreciate his help and patience to teach me how to be a better researcher. He provided insightful thoughts and suggestions along the way of the research project. His vision on how he drove the project forward to a challenging and exciting problems inspired me to investigate new experimental designs to tackle research problems.

Next, I would like to thank my committee members for their advices and discussions about my research project: Professor Javier Read de Alaniz, Professor Frederick W. Dahlquist, and Professor Kevin W. Plaxco. Through these advices, I obtained a lot of valuable comments and perspectives from the committee members on the future research directions.

My research project could not be completed without helps from a group of people from Nanyang Technological University (NTU) in Singapore: Dr. Cheng Zhou, Dr. Jamie Hinks, Dr. Gayatri Shankar Chilambi, Dr. Thomas Seviour, Yang Liu, and Professor Yuguang Mu. I had spent time learning and doing experiments in their laboratories for three weeks. They were very welcoming and helpful. I was grateful to work with them during my visit.

Another group of amazing people includes Alex Moreland, Samantha McCuskey, Dr. Hengjing Yan, Dr. Stephanie Fronk, Dr. Bing Wang, and Dr. Zach Rengert. I appreciate all of their supports both academically and mentally during my time in the Bazan group. I would not be able to make it though the project without them. They provided me countless useful science discussions and helped me through the process of getting started doing the

experiments in the lab, especially ones that were completely out of my comfort zone, *i.e.* biology-related experiments. Coming from organic synthesis group, it was challenging to start working with living organisms, but I made it through with their help.

I would like to acknowledge staffs and facilities of the Center for Polymers and Organic Solids (CPOS), Institute for Collaborative Biotechnologies (ICB), Department of Chemistry and Biochemistry, CNSI Biological Nanostructures Lab (BNL), and Materials Research Laboratory (MRL) as well as the funding from the ICB and Development and Promotion of Science and Technology Talents Project Scholarship (DPST) from the Institute for the Promotion of Teaching Science and Technology (IPST), Thailand.

Lastly, thanks to my family, my friends, and my roommates for their emotional support, especially during the first year of the graduate study. It was a great transition from an undergraduate program, and it took tremendous amount of efforts to adjust myself to a new environment with a fast-paced quarter system. None of my work would have been possible without them.

Abstract

Interactions of a Paracyclophane-based Conjugated Oligoelectrolyte with Biological Membranes

by

Jakkarin Limwongyut

A three-dimensional conjugated oligoelectrolyte (COE), COE2-3-pCp, was synthesized to study its effects on lipid bilayers. Its structure evolved from previously reported planar COEs via the incorporation of [2.2]paracyclophane within the delocalized central unit thus introducing an additional dimension to molecular format. The biological activity of COE2-3-pCp, in particular its insertion into and effects on biological membranes, was determined using both *in vitro* and molecular dynamic simulation techniques relative to its planar counterpart (COE2-3C). COE2-3-pCp induced higher lipid disorder, but without marked antimicrobial activity. In addition, COE2-3-pCp permeabilized lipid vesicles and cell membranes to an extent similar to that of COE2-3C. Combined, the data suggest that the non-inhibitory nature of COE2-3-pCp may result from a lower tendency to aggregate in the bilayer revealing that toxicity can be decoupled from membrane permeabilizing activity. Hence, subsequent generations of COEs may be designed to maximize membrane permeabilization while maintaining good biocompatibility for applications in whole-cell biocatalysis

Table of Contents

List of Figures

List of Tables

1. Introduction

Conjugated oligoelectrolytes (COEs) are defined by a conjugated backbone with ionic pendant groups tethered by hydrocarbon chains.[1,2] COEs typically intercalate within microbial membranes in a well-organized fashion.[3] Several molecular features are known to impact the extent of COE accumulation within cells and their effects on the membrane. For example, the degree to which the COEs intercalate within membranes depends on whether the charged groups are anionic or cationic.[4] Additionally, the number of repeat units affects the distortion of the lipid bilayer and is a strong modulator of antimicrobial efficacy.[5,6] Microbes with COEs have their properties and behavior modified in ways that are desirable for specific applications. Consider, the homologous series of oligophenylenevinylene COEs illustrated by DSBN+, DSSN+ and COE1-5C (Figure 1). While DSBN+ has higher antimicrobial efficacy than DSSN+, both increase membrane permeability in *E. coli* K12. COE1-5C, in contrast, has been shown to rigidify membranes.[5,7,8]

Oligophenylenevinylene COEs studied thus far largely contain a planar, two-dimensional conjugated fragment. A molecular structural variation that has yet to be considered concerns introducing dimensionality to the conjugated segment in order to understand possible repercussion of this structural modification on the reorganization of the membrane lipids and the overall perturbation of the bilayer. To accomplish this structural variation, we sought to include a rigid framework within the interior of the conjugated segment with an otherwise similar aspect ratio to phenylene unit. For this purpose, we chose the [2.2]paracyclophane (pCp) moiety. We hypothesized that three-dimensionality from the paracyclophane adduct would increase lipid disorder in the membrane. The structural evolution is illustrated in Figure 1.

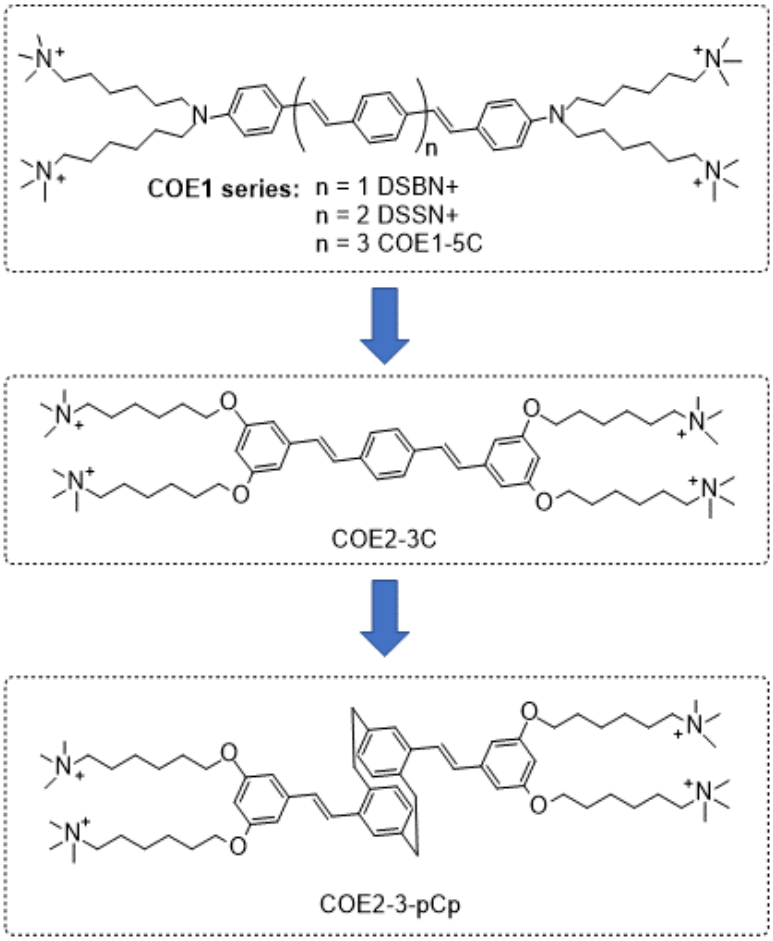

Figure 1. Structural evolution from the COE1 series to the paracyclophane-based COE (COE2-3-pCp). Iodide counterions are omitted from the structures.

We compared the properties of COE2-3-pCp to those of its linear counterpart COE2-3C by first carrying out molecular dynamics simulations to elucidate deformations and disorder within a model lipid bilayer structure. The results of the simulations provide a framework for understanding observed differences in the modification of *E. coli* K12 brought about by membrane modification with additional context provided by biophysical experiments with vesicles and cells. Of interest is the finding that while COE2-3-pCp has a lower minimum inhibitory concentration (MIC) relative to COE2-3C, it can induce similar levels of membrane permeabilization. Implications of increased permeabilization for whole-cell biocatalysis have been previously investigated using *E. coli* K12 and yeast (*S. cerevisiae*).[7,9,10]

2. Results and Discussion

The synthesis of COE2-3-pCp is shown in Figure 2. 4,16-Dibromo[2.2]paracyclophane (**1**), a pseudo-para isomer of dibromo[2.2]paracyclophane, was used as the key starting material to maintain the overall linearity of the backbone. Compound **1** was converted into **2** by using *s*-BuLi, followed by addition of *N*,*N*-dimethylformamide (DMF). Formyl groups were then subjected to reduction and chlorination with sodium borohydride and thionyl chloride, respectively, to yield **4**. The intermediate **5** was synthesized using triethyl phosphite. Precursor **7** was prepared under Horner-Wadsworth-Emmons (HWE) reaction conditions from **5** and **6**. Finally, treatment of **7** with trimethylamine provides COE2-3-pCp. COE2-3C, which is the planar analog of COE2-3-pCp, was synthesized according to reported protocols.[2,6]

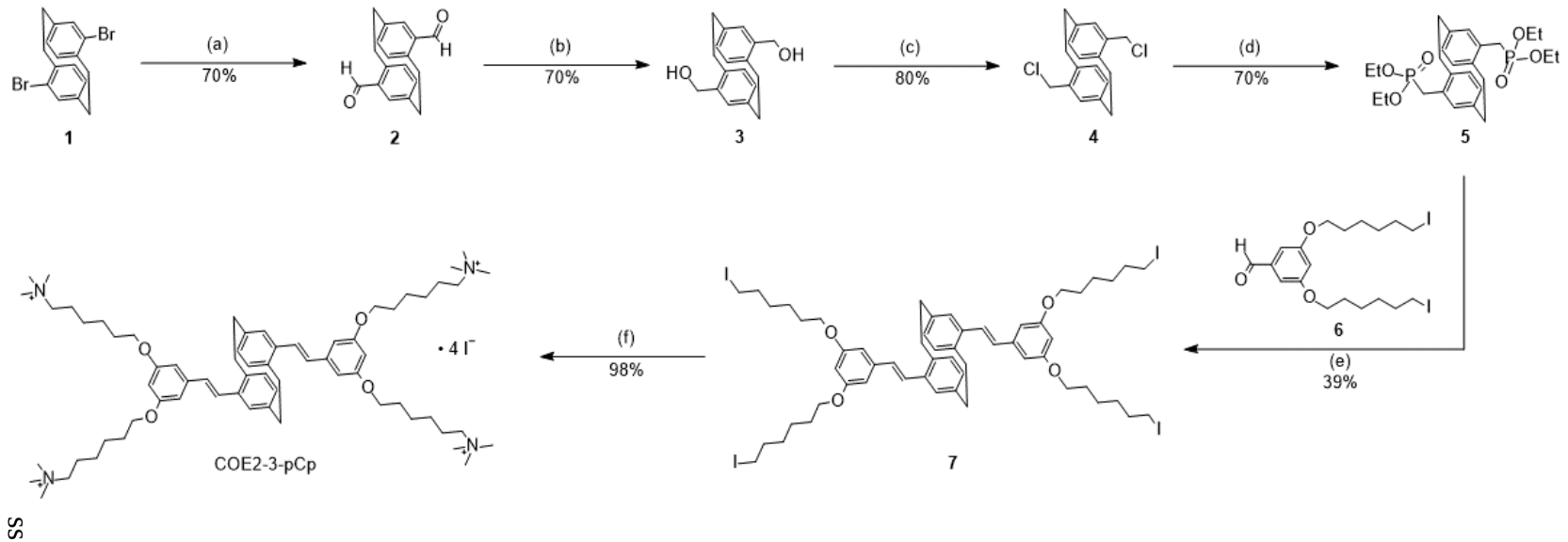

Figure 2. Synthesis of paracyclophane-based COE (COE2-3-pCp). Reaction conditions: (a) *s*-BuLi (2.3 equiv), DMF (10 equiv), THF, –78 °C to rt, 3 h; (b) $NaBH_4$ (3 equiv), EtOH/THF (1:5), rt, 3 h; (c) $SOCl_2$ (2.4 equiv), MeCN, 50 °C, 5 h; (d) $P(OEt)_3$, 135 °C, 48 h; (e) **6** (1.95 equiv), NaO^tBu (2.1 equiv), THF, rt, 6 h; (f) excess NMe_3, THF, MeOH, $CHCl_3$, rt, 48 h.

Absorption and fluorescence spectra of COE2-3-pCp are summarized in Appendix (Figure A1). The UV-visible absorption spectrum of COE2-3-pCp in water shows three absorption peaks in the ultraviolet region, namely, 225 nm, 311 nm and a shoulder peak at 328 nm. The COE2-3-pCp fluorescence exhibits an emission maximum at 436 nm. The emission maximum exhibits a hypsochromic shift of 15 nm when treated with a solution of 1,2-dimyristoyl-*sn*-glycero-3-phosphocholine (DMPC) vesicles. In previous studies, it was shown that when COEs intercalate into lipid bilayers, fluorescence emission will shift to shorter wavelength due to the change of environment from a polar (water) to a non-polar (lipid tails) environment. Hence, the observed shift in the emission of COE2-3-pCp in the vesicles suggests that COE2-3-pCp similarly intercalates into lipid membranes.[11]

To validate intercalation into lipid bilayers in microbes, *E. coli* K12 was treated with COE2-3-pCp in 50 mM phosphate buffer saline (PBS) at the turbidity of OD_{600} = 1. After staining, cells were centrifuged at 7000 rpm for 7 minutes and the supernatant was collected for UV-visible absorption measurements revealing more than 90% association of COE2-3-pCp to *E. coli* K12 cells, even when [COE2-3-pCp] = 40 μM (Figure 3a). Zeta potentials of cells and liposomes treated with COE2-3-pCp in 50 mM PBS were also measured (Figure 3b–c). An increase in zeta potential should be observed when COEs intercalate into the bilayers. However, while an increase was observed for liposomes, little change occurred with the cells (Figure 3b). The same observations were observed for COE2-3C with *E. coli* K12.[12] A plausible reason underlying the relatively constant zeta potential with *E. coli* may be the presence of the lipopolysaccharide (LPS) layer. With the thickness of the LPS being around 2–3 nm in *E. coli* K12, the COE cationic groups may not be able to reach the surface of the cells after their intercalation into the lipid bilayer due to the molecular length of the COEs.[12–14]

To verify COE2-3-pCp intercalation, we examined liposomes made of *E. coli* total lipid extract, which lacks the LPS layer. As shown in Figure 3c, the zeta potential increased with COE2-3-pCp concentration, indicating intercalation into the bilayer. Finally, to visually illustrate COE uptake, fluorescence signals in cell suspensions were imaged using two-photon microscopy. The images clearly show the accumulation of COE on the cells (Figure 4).

Molecular dynamics (MD) simulations were undertaken on Gram-negative model membrane bilayer systems (3:1 palmitoyloleoylphosphatidylethanolamine/palmitoyloleoylphospatidylglycerol, or POPE/POPG) doped with either COE2-3-pCp or COE2-3C (COE:POPE:POPG = 4:110:36). Relative to COE2-3C, COE2-3-pCp induced a greater degree of disorder, as illustrated by the more pronounced reduction in deuterium order parameter along the first fatty acid chain (sn1) of POPE predicted for COE2-3-pCp (Figure 5a). The same effect was observed on POPG for both the sn1 and sn2 (i.e. second fatty acid) chain. (Figure A3).

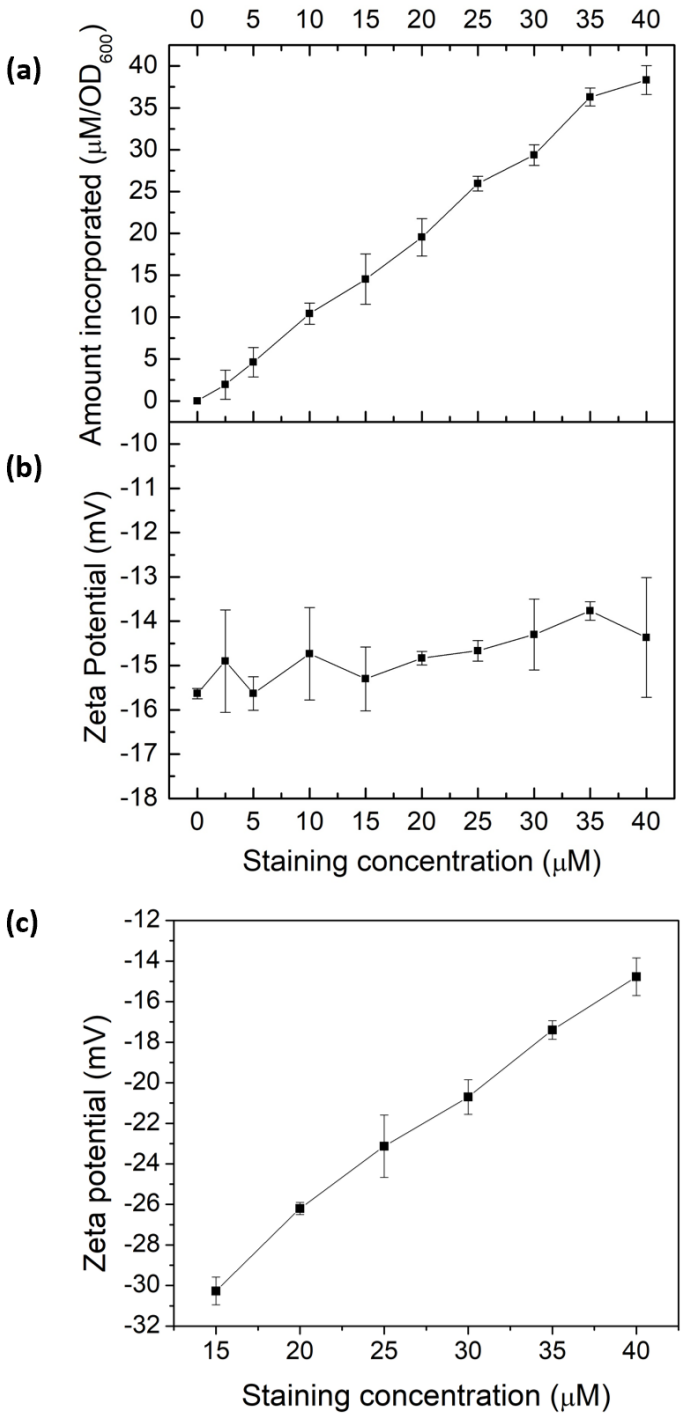

Figure 3. a) COE2-3-pCp association to *E. coli* K12 cells; zeta potential of (b) *E. coli* K12, and (c) *E. coli* total lipid extract vesicles at different COE2-3-pCp staining concentrations.

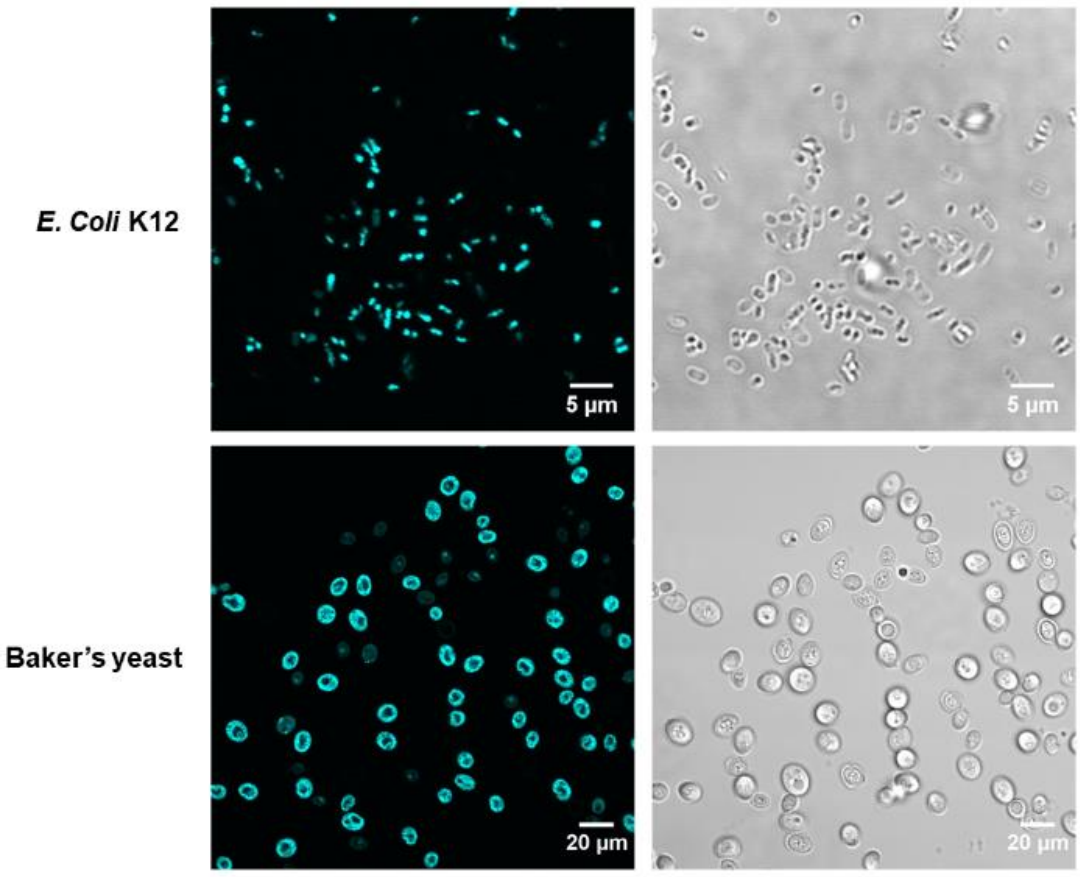

Figure 4. Two-photon micrographs of *E. coli* K12 and yeast treated with COE2-3-pCp from fluorescence channel (left) and brightfield channel (right). The excitation wavelength was 725 nm.

This increased disorder observed for COE2-3-pCp relative to COE2-3C resulted in a greater reduction of the average bilayer thickness of the COE2-3-pCp-doped lipid bilayer (Figure 5b). Earlier studies proposed that the COE length was a key parameter with regards to their antibiotic characteristics. Thus, antimicrobial activity was determined against *E. coli* K12 and yeast using broth microdilution method.[15] All experiments were performed in triplicate (Figure A2). Specifically, the minimum inhibitory concentrations (MICs) of COE2-3-pCp on *E. coli* K12 and yeast are 64 μM and 128 μM, respectively, whereas those of COE2-3C are 16 μM and 64 μM, respectively. Modification of the COE by introducing a three-dimensional moiety decreased inhibitory action despite reduction of bilayer thickness. Hinks et al. attributed a reduction in antimicrobial activity of a fluorinated COE to increased range of movement of the COE pendant arm, which reduced the mechanical shock to the lipid bilayer. Another effect of this increased lability was reduced molecular aggregation within the bilayer and it is possible that this also contributed to attenuating COE2-3-pCp driven membrane disruption.[5]

According to the probability distribution for intermolecular distance between each COE pair in a four COE simulation (see Appendix for definition) (Figure 5c), there was a 36% reduction in the duration that COE2-3-pCp molecules exist as an aggregate, relative to COE2-3C, as determined from an intermolecular distance of < 0.5 nm. While introducing a non-planar aspect to the design of COEs may increase disorder, MD simulations indicate that the effect of this with regards to antimicrobial activity is most reasonably offset by reduced aggregation.

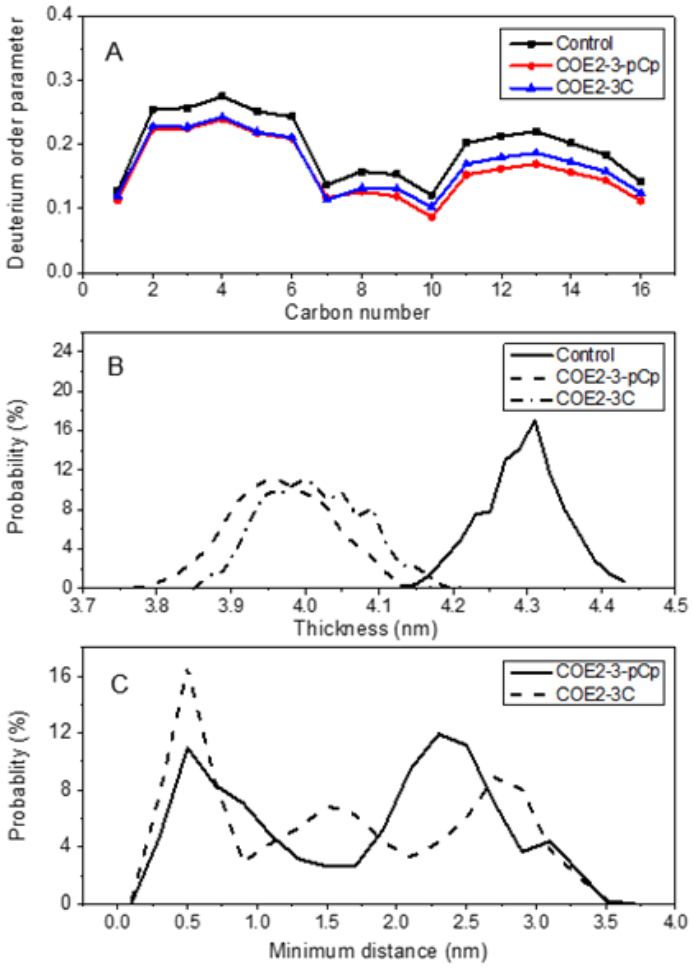

Figure 5. a) Local deuterium order parameter along the sn1 aliphatic chain of POPE for model bilayer system (122:40 POPE:POPG) only (i.e. control), and with either COE2-3-pCp or COE2-3C (4:110:36, COE:POPE:POPG). b) Probability distribution function for average bilayer thickness for the model bilayer system only (122:40 POPE:POPG), and with either COE2-3-pCp or COE2-3C (4:110:36, COE:POPE:POPG) based on the center of mass distance between phosphorous atoms in the two leaflets. c) Probability distribution function of minimum bridging distance between each pair of dopant molecules in model bilayer system simulations with either COE2-3-pCp or COE2-3C (4:110:36, COE:POPE:POPG). The data were averaged across the last 50 ns of 3 × 200 ns simulations.

COE permeabilization ability was determined by calcein released from *E. coli* total lipid extract vesicles treated with the two COEs. At the COE amount of 2.5 mol% relative to lipids, COE2-3-pCp induced leakage up to 25% in 100 minutes, while COE2-3C induced 16% within the same timeframe (Figure 6a). This supports the hypothesis that COE2-3-pCp has a potential to be a more effective membrane permeabilizer.

The impact of COEs on whole-cell biocatalysis was investigated using *E. coli* K12 hydrolysis of *o*-nitrophenyl β-D-galactopyranoside (ONPG) by β-galactosidase.[16,17] Cells treated with COEs show increased catalytic rates. Turnover rates are 2.8 and 2.3-fold faster than untreated cells upon treatment with 25 μM COE2-3-pCp and COE2-3C, respectively (Figure 6b). With the higher MIC of COE2-3-pCp compared to COE2-3C toward *E. coli* K12, the degree to which association with COEs impacts cell viability can thus be decoupled from the ability to permeabilize the membrane. Such an observation is surprising since these two properties usually follow the same trend.[18]

The membrane permeabilization effect was also tested with yeast. Relative extracellular ATP levels were used as an indicator of permeabilization as previously described.[19] The amount of ATP in the supernatant is directly proportional to the observed luminescence signal from the luciferase-luciferin system. Yeast treated with 100 μM of COEs show higher extracellular ATP than control, indicating permeabilization (Figure 7a).

The enantioselective hydration of fumarate by fumarase was then chosen for a model system to monitor biocatalysis, as the turnover rate can be accelerated by increasing permeability.[20] Yeast cells were treated with 25 μM COEs per 0.1 g wet cells. Cells with COE2-3-pCp show significant catalytic acceleration from untreated cells at comparable degree to those treated with COE2-3C (Figure 7b). Despite the slightly higher permeabilizing efficacy of COE2-3-pCp on *E. coli* K12, COE2-3-pCp is slightly less

effective with yeast. Such differences may be related to the differences in membrane composition, but a more precise mechanistic rationale requires further work.

3. Conclusion

In summary, the paracyclophane-based COE2-3-pCp was designed and synthesized. Despite its similar length and cell association profile to its linear counterpart COE2-3C, COE2-3-pCp exhibits a higher MIC towards *E. coli* K12 and yeast. Moreover, COE2-3-pCp permeabilizes lipid bilayers to a similar extent as COE2-3C and thus improves biocatalysis processes in both microorganisms relative to untreated cells. In contrast to the higher MIC of COE2-3-pCp compared to COE2-3C, MD simulation suggests the paracyclophane unit introduces more lipid disorder with higher extent of membrane thinning. Perhaps more surprisingly, the general molecular topology of COE2-3-pCp reduces the tendency to form aggregates in the membrane. To what degree self-association of COEs within the membrane impacts their ability to reduce cell viability remains an open question right now due to the absence of relevant experimental techniques. These insights hint to the strategic design of new COEs to manipulate intermolecular interactions that attenuate inhibition, while inducing permeabilization—findings that are relevant within the context of whole-cell biocatalysis.

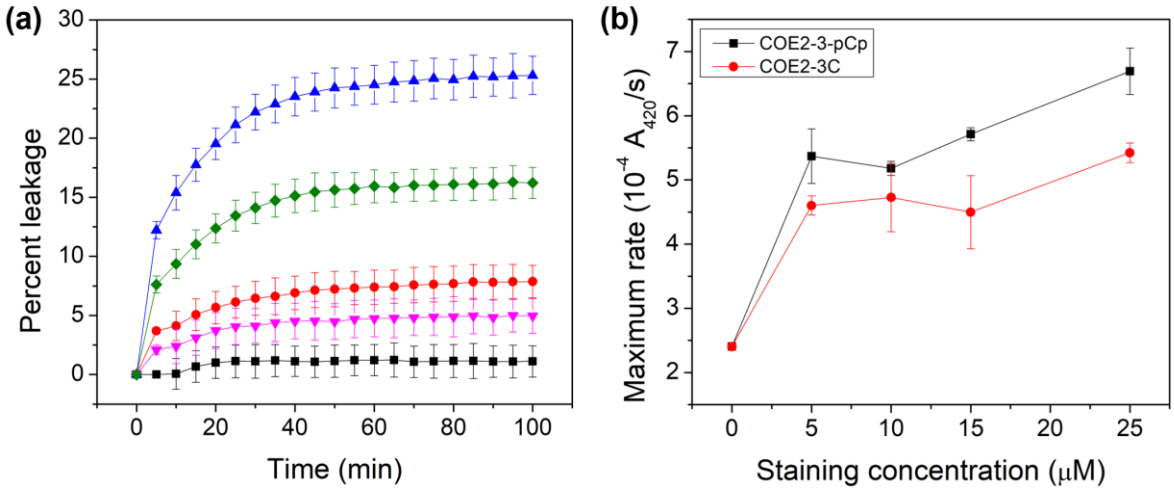

Figure 6. a) Leakage of calcein from *E. coli* total lipid extract vesicles over time. (Legend: ▲ = 2.5 mol% COE2-3-pCp, ● = 1 mol% COE2-3-pCp, ♦ = 2.5 mol% COE2-3C, ▼ = 1 mol% COE2-3C, ■ = control), b) Rate of ONPG hydrolysis at different staining concentration in *E. coli* K12

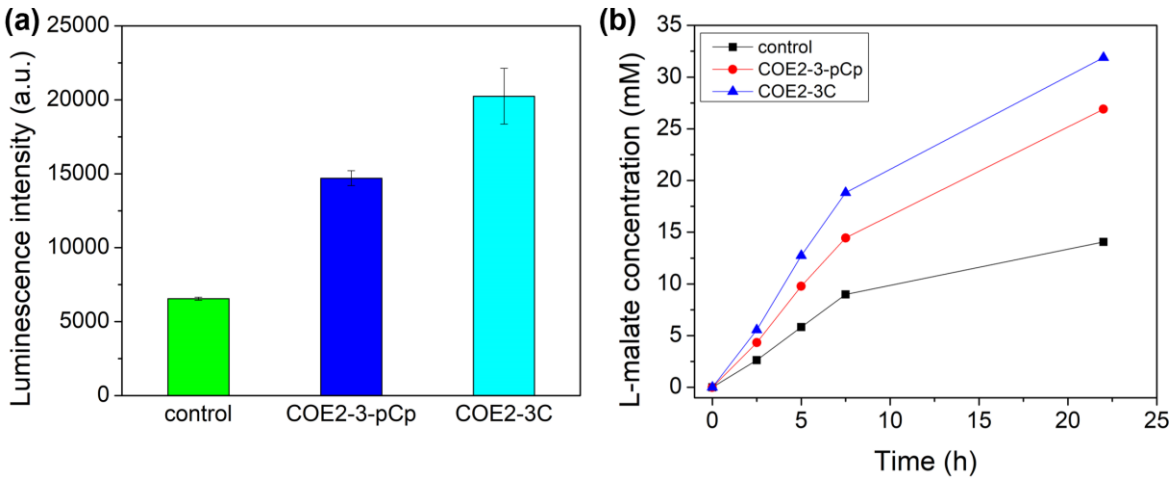

Figure 7. a) Luminescence intensity obtained from extracellular ATP assay with supernatants from yeast cells treated with the COEs, b) concentration of L-malate produced by yeast over time. Yeast cells were stained with 25 µM of the indicated COEs.

Appendix

1. Materials and Instruments

All chemicals and solvents were purchased from Sigma-Aldrich, Fisher Scientific, Alfa Aesar, Acros, and 1-Materials and used as received without further purification unless otherwise stated. Tetrahydrofuran (THF) and *N*,*N*-dimethylformamide (DMF) was purified and dried under solvent purification system. Water was purified using a MilliQ Plus System (Millipore Corporation) to the resistivity of 18 MΩ.cm. Analytical thin layer chromatography was performed using Merck aluminum plate pre-coated with silica gel 60 F254. Flash column chromatography was carried out using silica gel Silicycle SiliaFlash P60 (230-400 mesh). UV-visible absorption spectrum was recorded using Perkin Elmer Lambda 750 spectrometer. Fluorescence spectra were recorded using PTI Quanta Master spectrofluorometer. Nuclear magnetic resonance (NMR) spectra were recorded on a Varian 500 MHz or Varian 600 MHz spectrometers. Cell imaging were performed using an Olympus Fluoview 1000MPE Multiphoton/Laser Scanning Confocal microscope.

2. Synthesis

2.1 Synthesis of 4,16-diformyl[2.2]paracyclophane (2)

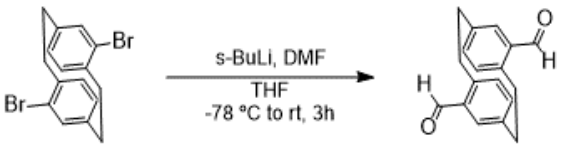

To a dry round bottom flask was charged with 4,16-dibromo[2.2]paracyclophane (**1**) (600 mg, 1.64 mmol) under argon and 36 mL of dry THF was added. The resulting

suspension was stirred and cooled down to –78 °C. Then, *s*-BuLi (1.6 M in cyclohexane) (2.36 mL, 3.77 mmol) was added via syringe. The reaction mixture immediately turned yellow. The solution was stirred at –78 °C for an hour to ensure complete lithiation. Afterward, 0.6 mL of dry DMF was added. The resulting mixture was heated up to room temperature and kept stirring for 3 hours. Dilute HCl (1 M) was added afterward to quench the reaction. The solution was diluted with dichloromethane, washed with saturated sodium bicarbonate solution followed by brine. Combined organics were dried over Na_2SO_4. Solvent was removed under reduced pressure. Crude mixture was purified by column chromatography using 2:8 ethyl acetate/hexane as an eluent to obtain white solid (303 mg, 70%).

^{1}H NMR (600 MHz, $CDCl_3$): δ (ppm) = 9.94 (s, 2H), 7.05 (d, 2H, *J* = 2.0 Hz), 6.63 (dd, 2H, *J* = 7.7 Hz, *J* = 2.0 Hz), 6.52 (d, 2H, *J* = 7.7 Hz), 4.15–4.11 (m, 2H), 3.31–3.27 (m, 2H), 3.18–3.13 (m, 2H), 3.04–2.99 (m, 2H); ^{13}C NMR (150 MHz, $CDCl_3$): δ (ppm) = 192.04, 143.05, 140.67, 137.11, 136.93, 136.68, 135.38, 34.51, 32.96; HRMS (ESI) *m/z* calcd for $C_{18}H_{16}O_2$: 264.1150, found: 264.1160 $[M]^+$.

2.2 Synthesis of 4,16-di(hydroxymethyl)[2.2]paracyclophane (3)

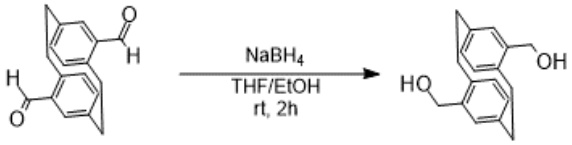

To a dry round bottom flask was charged with **2** (200 mg, 0.757 mmol). 20 mL of THF was later added and the mixture was stirred until all solid dissolved. In a separate flask, $NaBH_4$ (86 mg, 2.27 mmol) was added under inert atmosphere and dissolved in 1 mL of ethanol. The ethanolic solution was immediately transferred to the reaction flask via syringe.

The reaction mixture was stirred at room temperature for 2 hours. After reaction completion indicated by TLC, dilute HCl (1 M) was added dropwise to quench any leftover reagent. The resulting mixture was diluted with ethyl acetate, washed with saturated sodium bicarbonate solution and brine. Combined organic phase was dried over Na_2SO_4. Solvent was removed using rotary evaporator. Crude mixture was recrystallized in ethyl acetate/hexane solvent system to yield compound **3** as white powder (142 mg, 70%).

^{1}H NMR (600 MHz, methanol-d4): δ (ppm) = 6.63 (dd, 2H, *J* = 7.7 Hz, *J* = 1.9 Hz), 6.41 (d, 2H, *J* = 1.9 Hz), 6.35 (d, 2H, *J* = 7.7 Hz), 4.69 (d, 2H, *J* = 13.0 Hz), 4.36 (d, 2H, *J* = 13.0 Hz), 3.41–3.37 (m, 2H), 3.10–3.01 (m, 4H), 2.88–2.83 (m, 2H); ^{13}C NMR (150 MHz, methanol-d4): δ (ppm) = 141.42, 140.75, 138.48, 135.03, 133.84, 129.13, 64.62, 34.60, 33.12; HRMS (ESI) *m/z* calcd for $C_{18}H_{20}O_2$: 268.1463, found: 268.1472 $[M]^+$.

2.3 Synthesis of 4,16-di(chloromethyl)[2.2]paracyclophane (4)

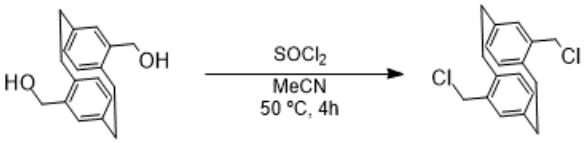

A suspension of **3** (100 mg, 0.373 mmol) in 5 mL of acetonitrile was stirred in a flame-dried round bottom flask under argon. Then, $SOCl_2$ (0.065 mL, 0.894 mmol) was slowly added to the suspension using a syringe. The resulting mixture was stirred under argon at 50 °C for 4 hours. Excess $SOCl_2$ was quenched via addition of water after the solution cooled down to room temperature. The solution was diluted using dichloromethane, washed with saturated sodium bicarbonate solution and brine. Organic phases were dried over Na_2SO_4. Solvent was removed using rotary evaporator. Crude mixture was recrystallized in dichloromethane/methanol solvent system to yield **4** as white crystalline solid (91 mg, 80%).

^{1}H NMR (600 MHz, $CDCl_3$): δ (ppm) = 6.61 (dd, 2H, *J* = 7.8 Hz, *J* = 1.9 Hz), 6.42 (d, 2H, *J* = 1.9 Hz), 6.38 (d, 2H, *J* = 7.7 Hz), 4.58 (d, 2H, *J* = 11.8 Hz), 4.32 (d, 2H, *J* = 11.8 Hz), 3.46–3.41 (m, 2H), 3.14–3.03 (m, 4H), 2.95–2.90 (m, 2H); ^{13}C NMR (150 MHz, $CDCl_3$): δ (ppm) = 139.97, 138.17, 136.58, 134.65, 134.44, 130.10, 45.62, 33.94, 32.47; HRMS (ESI) *m/z* calcd for $C_{18}H_{18}Cl_2$: 304.0786, found: 304.0791 $[M]^+$.

2.4 Synthesis of tetraethyl 4,16-bismethylene[2.2]paracyclophanebisphosphonate (5)

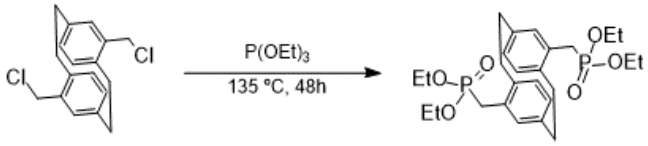

To a dry gas-tight vessel was charged with **4** (142 mg, 0.465 mmol) and 2 mL of $P(OEt)_3$. The vessel was sealed, and the resulting suspension was stirred at 135 °C for 48 hours. After that, the solution was cooled down to room temperature. Precipitates were vacuumed filtered and recrystallized in hot toluene to obtain compound **5** as white crystalline solid (166 mg, 70%).

^{1}H NMR (600 MHz, $CDCl_3$): δ (ppm) = 6.61 (dt, 2H, *J* = 7.9 Hz, *J* = 2.0 Hz), 6.35 (dd, 2H, *J* = 7.9 Hz, *J* = 1.6 Hz), 6.19 (t, 2H, *J* = 1.9 Hz), 3.93–3.82 (m, 8H), 3.48–3.43 (m, 2H), 3.12 (dd, *J* = 14.8 Hz, *J* = 22.0 Hz), 3.08–3.04 (m, 2H), 2.97–2.92 (m, 2H), 2.83 (dd, *J* = 14.8 Hz, *J* = 21.8 Hz), 2.82–2.77 (m, 2H), 1.15 (td, *J* = 7.0 Hz, *J* = 0.8 Hz); ^{13}C NMR (150 MHz, $CDCl_3$): δ (ppm) = 139.30, 139.28, 138.27, 138.23, 136.76, 136.72, 133.82, 133.80, 131.18, 131.12, 127.42, 127.40, 62.12, 62.08, 62.03, 61.99, 33.24, 33.21, 33.12, 32.32, 16.30, 16.25 (Most peaks appear as doublets which may be caused by C–P couplings); HRMS (ESI) *m/z* calcd for $C_{26}H_{38}O_6P_2Na$: 531.2042, found: 531.2046 $[M+Na]^+$.

2.5 Synthesis of 7

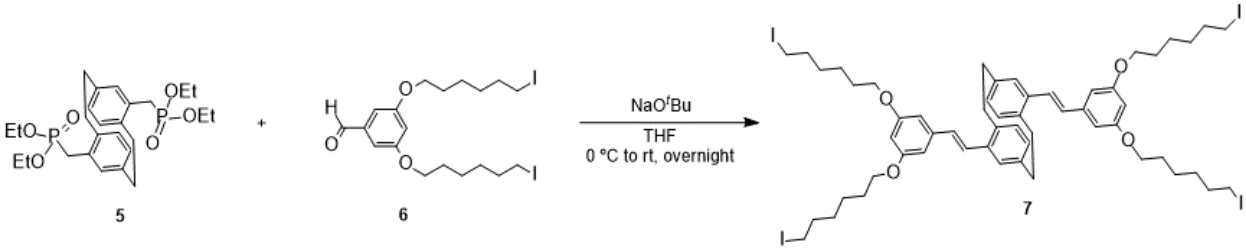

5 6 7

A flame-dried round bottom flask was charged with a Teflon-coated magnetic stir bar, **5** (80 mg, 0.157 mmol), 3,5-bis(6-iodohexyloxy)benzaldehyde (**6**) (171 mg, 0.307 mmol). Anhydrous THF was later added to the flask to dissolve compounds. The resulting solution was cooled down to 0 ˚C in an ice bath. Sodium *tert*-butoxide (32 mg, 0.330 mmol) was taken out of the glovebox in a round-bottom flask and was connected to Schlenk manifold. THF was added to the base and the resulting solution was immediately transferred to the reaction flask via syringe. After complete addition of the base, the reaction was heated up to room temperature and stirred overnight. The mixture was then diluted with dichloromethane, washed with water and brine, dried over Na_2SO_4, and concentrated *in vacuo*. Crude reaction mixture was purified by column chromatography using 1:1 dichloromethane/hexane as an eluent to yield **7** as white powder (81 mg, 39%)

^{1}H NMR (600 MHz, $CDCl_3$): δ (ppm) = 7.16 (d, 2H, *J* = 16.2 Hz), 6.78 (d, 2H, *J* = 16.2 Hz), 6.71 (d, 4H, *J* = 2.4 Hz), 6.66–6.64 (m, 4H), 6.42–6.40 (m, 4H), 4.02 (t, 8H, *J* = 6.6 Hz), 3.56 (t, 2H, *J* = 13.2 Hz), 3.22 (t, 8H, *J* = 7.2 Hz), 3.08 (t, 2H, *J* = 13.2 Hz), 3.02–2.97 (m, 2H), 2.94–2.89 (m, 2H), 1.91-1.82 (m, 16H), 1.57–1.50 (m, 16H); ^{13}C NMR (150 MHz, $CDCl_3$): δ (ppm) = 160.62, 140.02, 139.60, 138.40, 137.37, 133.70, 130.36, 129.71, 129.56, 127.60, 105.41, 100.62, 68.02, 34.65, 33.56, 33.52, 30.42, 29.28, 25.29, 7.16; MS (FD) calcd for: 1316.16, found: 1316.2.

2.6 Synthesis of COE2-3-pCp

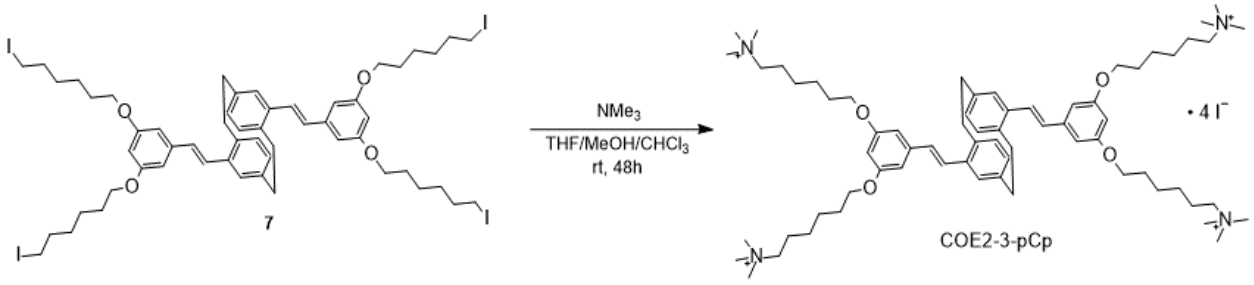

To a round-bottom flask charged with a magnetic stir bar was added **7** (68 mg, 0.052 mmol) under argon. 5 mL of dry THF was added to dissolve all of the solid. Then, a 3.2 M methanolic solution of trimethylamine (0.16 mL, 0.520 mmol) was added via a syringe. The resulting solution was stirred at room temperature for 48 hours. Small portions of chloroform were later added to the flask periodically to dissolve any precipitates formed during the course of the reaction. Organic solvents were removed under reduced pressure and deionized water was added to the flask to dissolve the desired compound. The aqueous solution was filtered through 0.2 µm filter and freeze dried to yield COE2-3-pCp as white fluffy solid (79 mg, 98%).

^{1}H NMR (500 MHz, DMSO-d6): δ (ppm) = 7.26 (d, 2H, *J* = 16.1 Hz), 6.90 (d, 2H, *J* = 16.1 Hz), 6.84 (s, 4H), 6.74 (s, 2H), 6.52 (d, 2H, *J* = 7.7 Hz), 6.44 (d, 2H, J = 7.7 Hz), 6.42 (s, 2H), 4.03 (t, 8H, *J* = 6.4 Hz), 3.63–3.61 (m, 2H), 3.06 (s, 36H), 2.92–2.88 (m, 6H), 1.80–1.70 (m, 16H), 1.55–1.49 (m, 8H), 1.40–1.34 (m, 8H); ^{13}C NMR (125 MHz, DMSO-d6): δ (ppm) = 160.05, 139.63. 139.11, 138.17, 137.06, 133.41, 129.92, 129.23, 129.09, 127.15, 105.12, 100.36, 67.39, 65.27, 52.44, 52.21, 52.18, 34.00, 32.69, 28.51, 25.51, 25.12, 22.04; HRMS (ESI) *m/z* calcd for $[C_{68}H_{108}N_4O_4I_2]^{2+}$: 649.3230, found: 649.3230 $[M\text{-}2I]^{2+}$.

3. Photophysical Properties Measurements

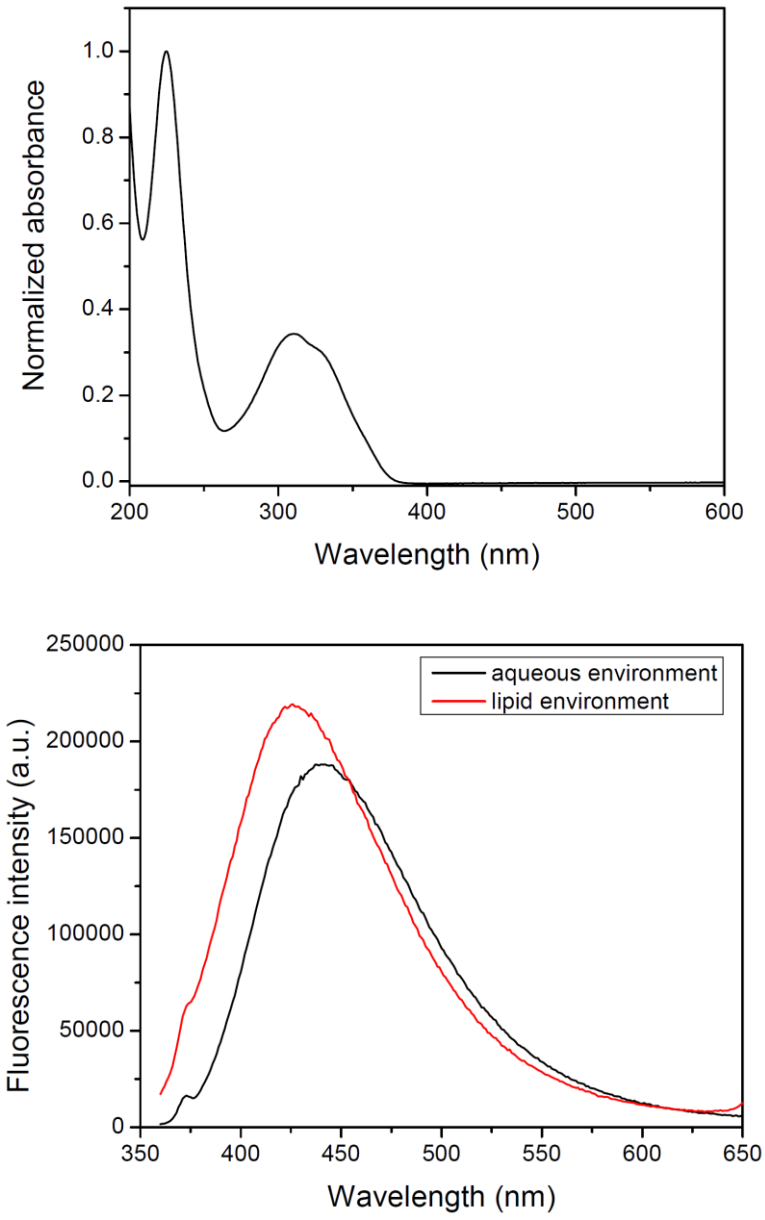

Figure A1. (top) UV-Visible absorption spectrum of COE2-3-pCp in water; (bottom) fluorescence spectra of COE2-3-pCp in water (black trend) and when it intercalated into DMPC vesicles (red trend).

Table A1. Absorption maxima of COE2-3-pCp in water and their molar extinction coefficients (ε).

Absorption maximum (λ_{max} / nm)	Molar extinction coefficient (ε / 10^4 $M^{-1}cm^{-1}$)
225	12.5
311	4.3
328	3.8

4. Experimental Details

Cell Culture

A single colony of *E. coli* K12 (ATCC 10798) from an agar plate was cultured in Lysogeny broth (10 g bacto tryptone, 5 g yeast extract, 10 g NaCl in 1 L water) at 37 °C. Yeast (*S. cerevisiae*) was bought from a local grocery store and rehydrated in yeast selective growth medium (40 g dextrose, 10 g casaminoacids, 3.4 g yeast nitrogen base without $(NH_4)_2SO_4$ and amino acids, 10.6 g $(NH_4)_2SO_4$, 2.7 g Na_2HPO_4, 4.28 g NaH_2PO_4, 100 mg Pen/Strep/Neo, 20 mg Amp, and 20 mg Kan in 1 L water) or 0.1 M neutral phosphate buffer at 30 °C with 200 rpm shaking.

Cell Association Assay

A single colony of *E. coli* K12 from a plate culture was inoculated in LB at 37 °C and harvested at log phase. Cells were pelleted by centrifugation at 7000 rpm for 7 minutes and washed with 50 mM PBS. The cells were then resuspended in 50 mM PBS until reach an OD_{600} of 2 by extrapolation. Then, 500 µL of the cell suspension was mixed with 500 µL of COE solution in the same buffer at different concentrations. After incubation at 30 °C for 1.5

hours, the mixtures were centrifuged at 7000 rpm for 7 minutes. Supernatant from each sample was collected and measured residual absorbance from COE2-3-pCp at 325 nm using Tecan Infinite M200 Plate Reader.

Zeta Potential Measurements of *E. coli* K12 cells

E. coli K12 suspension in 50 mM PBS at OD_{600} of 2 was prepared using the same protocol for cell association assay above. 500 µL of the suspension was mixed with 500 µL of COE solution at desired concentrations. The mixtures of COE and cells were then incubated at 30 °C for 1.5 hours. After incubation, the mixtures were diluted 10-fold. The diluted solutions were used for zeta potential measurements by Zeta Sizer Nano ZS (Malvern Panalytical Inc.)

Zeta Potential Measurements of *E. coli* total lipid extract vesicles

E. coli total lipid extract (Avanti Polar Lipids) was weighed in a vial, dissolved in chloroform. The lipid solution was dried using rotary evaporator and put under high vacuum overnight. The lipid film was kept at –20 °C until use. Prepared lipid film was taken out of a freezer and warmed up to room temperature. Then, 50 mM PBS was added to resuspend the lipid. The resulting suspension was extruded through 0.2 µm polycarbonate filter (Whatman) 11 times, followed by 0.1 µm polycarbonate filter (Whatman) 11 times. Freshly prepared vesicles were diluted with the buffer and treated with COE2-3-pCp at different final COE concentrations. The final concentration of lipid vesicles was 3 mg/mL. The vesicles were then incubated at 30 °C for 1 hour and were sample out for zeta potential measurements using Zeta Sizer Nano ZS (Malvern Panalytical Inc.)

Minimum Inhibitory Concentration Experiments

MIC Experiments were performed based on broth microdilution method on 96-well plates. For *E. coli* K12, cells were inoculated and collected during late log phase. Cell suspension was diluted down in LB to reach 1×10^6 cfu/mL. The resulting suspension was mixed with different concentrations of COE2-3-pCp and COE2-3C in a 96-well plate (Thermo Fisher). The plate was incubated overnight at 37 °C with 200 rpm shaking. For yeast, yeast cells were rehydrated according to the aforementioned protocol and diluted down in yeast selective growth medium to OD_{600} = 0.04. The resulting suspension was mixed with different concentrations of COE2-3-pCp and COE2-3C in a 96-well plate (Thermo Fisher). The plate was incubated overnight at 30 °C with 200 rpm shaking for two days. MICs were determined as the lowest concentration of COEs that inhibit visible growth of microorganisms. All experiments were performed in triplicate.

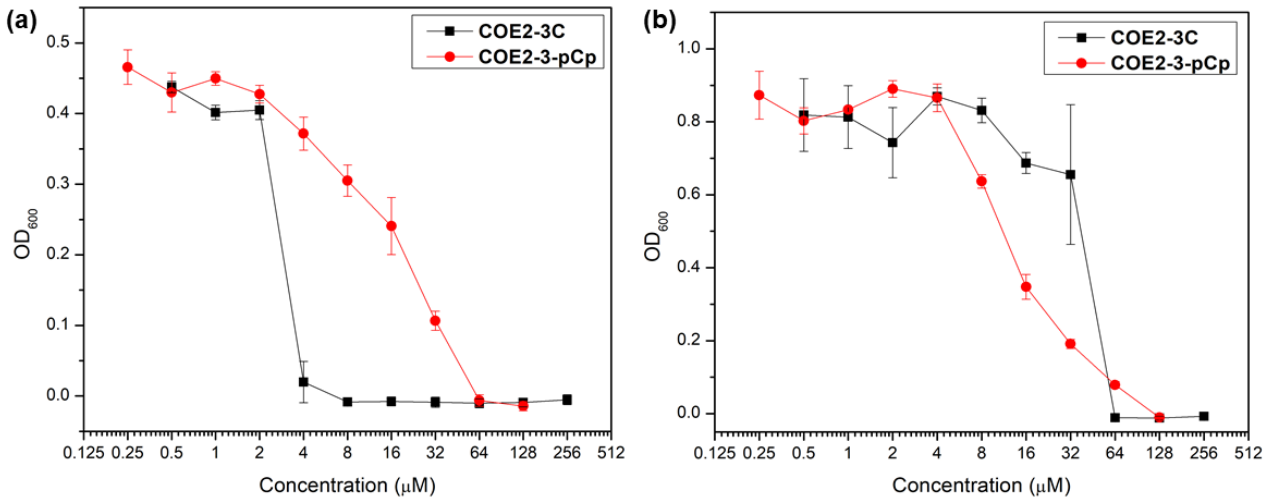

Figure A2. Final OD_{600} of (a) *E. coli* K12 and (b) yeast after the incubation with different concentration of COE2-3C and COE2-3-pCp. MICs are defined as the lowest COE concentration that no growth of microorganisms was observed.

ONPG Turnover Assay by *E. coli* K12

A single colony of *E. coli* K12 was inoculated in LB supplemented with 2% lactose to induce *lacZ* expression at 37 °C overnight with 200 rpm shaking. Cell suspension was then centrifuged at 7000 rpm for 7 minutes to remove the growth medium and washed with M9 minimal salt solution. The cells were resuspended and treated with different concentration of COEs in M9 minimal salt solution at the final turbidity of 0.6 OD_{600} for 1.5 hours at 30 °C. Then the cells were centrifuged, washed and resuspended. In a 96-well plate (Thermo Fisher), 100 µL of bacteria suspension, 3.9 mM ONPG solution, and M9 salt solution were mixed together and the absorbance was measured at 420 nm every 5 minutes for 90 minutes at 37 °C using a Tecan Infinite M200 Plate Reader.

Extracellular ATP Assay

The extracellular ATP was quantified as a measure of the membrane damage by COE2-3-pCp and COE2-3C. Yeast was rehydrated in 0.1 M neutral phosphate buffer at 30 °C for 1 hour and washed with the buffer. Then, 0.1 g of wet yeast were weighed in clean centrifuge tube and resuspended with 4 mL of the buffer. The yeast was treated with 100 µM of COEs for 120 minutes at 30 °C. An equal volume of buffer was added in the untreated control. After COE treatment, samples were centrifuged at 4000 × g for 10 min and the supernatant was collected to determine the extracellular ATP concentration. 100 µL of sample was added to 100 µl of BacTiter Glo reagent in a 96-well plate (Corning). After 5 minutes of incubation, the luminescence was measured using a Tecan infinite pro M200 microplate reader. Samples were taken in triplicate and standard deviation was measured. The luminescence was proportional to the amount of extracellular ATP released after membrane damage in the samples.

Fumarate Conversion by Yeast

In a centrifuge tube with 2 mL of a warm 0.1 M phosphate buffer, 0.3 g of dry yeast cells were suspended, and 12 mL of yeast selective media were added. Cell suspension was incubated at 30 °C overnight with 200 rpm shaking. After the incubation, the cells were pelleted and washed with the buffer. 0.1 g of wet yeast was used in each reaction tube. The wet yeast cells were treated with 25 μM of COEs in the buffer (4 mL) at 30 °C for 2 hours. The buffer without any COE was added to the untreated control tube. After that, cells were centrifuged, washed, and resuspended in the buffer containing 50 mM fumaric acid. The tubes were incubated at 30 °C with 200 rpm shaking. Supernatants were sampled at 2.5, 5, 7.5, and 22 hours of incubation. The aliquots were filtered through 0.22 μm PFTE filter (Thermo Fisher) and diluted 10-fold in an eluent. Amount of L-malate presented in the aliquots was then analyzed by HPLC using a Shimadzu UFLC instrument SIL-20AHT with an organic acid compatible C18 Kinetix column 2.6 μM FS 100A 150 × 4.6 mm. (Pheonomenex). The eluent was 20 mM potassium phosphate pH 2.0 with the flow rate of 1.25 mL/min.

5. Molecular Dynamics Simulations

All the Molecular Dynamics (MD) simulations were carried out by Gromacs 4.6.7 package.[21] CHARMM general force field[22] and CHARMM36 lipid force field[23] were used to characterize the COE molecules and the lipid molecules, respectively. Totally three different systems were simulated in this study (200 ns × 3 repeats), the pure lipid bilayer (referred as control), the lipid bilayer embedded with COE2-3-pCp molecules (referred as COE2-3-pCp), and the lipid bilayer embedded with COE2-3C molecules (referred as COE2-3C). The pure

lipid bilayer was modeled as a generalized Gram-negative bacterial inner membrane, which contains POPE and POPG with a ratio 122:40. After 200 ns simulation, the last frame was used to build up the COE-embedded bilayers. 6 POPE molecules and 2 POPG molecules were removed from each leaflet of the bilayer to insert 4 COE molecules. The final model (COE:POPE:POPG equals to 4:110:36) is equilibrated for another 50 ns with position restraints of COE molecules before the production run. During the simulation, a leap-frog algorithm was used to integrate Newton's equation of motion, and the time step was set to 2 fs. The Na^+ and Cl^- ions were added to TIP3P water model[24] to neutralize the system and reach a concentration of a 0.15 M physiological salt solution. All the covalent bonds in solutes and solvents were constrained by the LINCS algorithm[25] and the SETTLE algorithm,[26] respectively. The simulations were performed in NPT ensemble with the temperature of 310 K and pressure of 1 bar. The Nose-Hoover algorithm[27] and the semi-isotropic Parrinello-Rahman algorithm[28] were used for the temperature coupling and the pressure coupling. The cut-off for the short-range electrostatics and Lennard-Jones interactions were both set as 1.2 nm and the particle mesh Ewald (PME)[29] algorithm was used to calculate the long-range electrostatic interactions.

The intermolecular distance is defined as the minimum atom-distance in one COE-pair. Two COE molecules are considered contacted if this distance is smaller than 0.5 nm. Four COE molecules lead to six different COE-pairs. The last 50 ns trajectories of the three repeats were used for the statistics. Based on the results, the contacting probability of two COE2-3-pCp molecules is 15.75%, while that of two COE2-3C molecules is 24.57%.

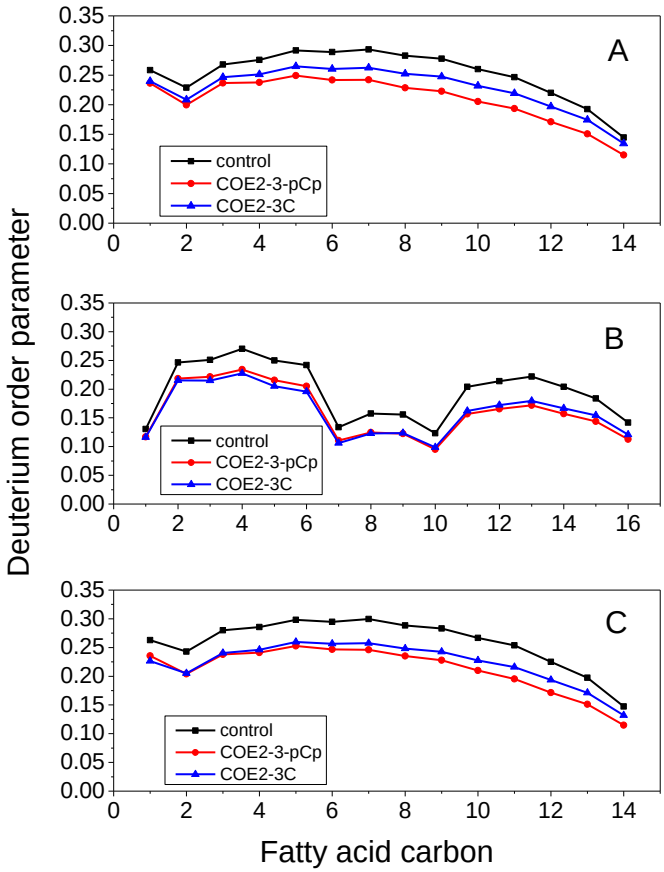

Figure A3. a) Local deuterium order parameter along the sn2 aliphatic chain of POPE for model bilayer system (122:40 POPE:POPG) only (i.e. control), and with either COE2-3-pCp or COE2-3C (4:110:36, COE:POPE:POPG) b) Local deuterium order parameter along the sn1 aliphatic chain of POPG for model bilayer system (122:40 POPE:POPG) only (i.e. control), and with either COE2-3-pCp or COE2-3C (4:110:36, COE:POPE:POPG) c) Local deuterium order parameter along the sn2 aliphatic chain of POPG for model bilayer system (122:40 POPE:POPG) only (i.e. control), and with either COE2-3-pCp or COE2-3C (4:110:36, COE:POPE:POPG). The data were averaged across the last 50 ns of 3 × 200 ns simulations.

6. NMR Spectra of Synthesized Compounds

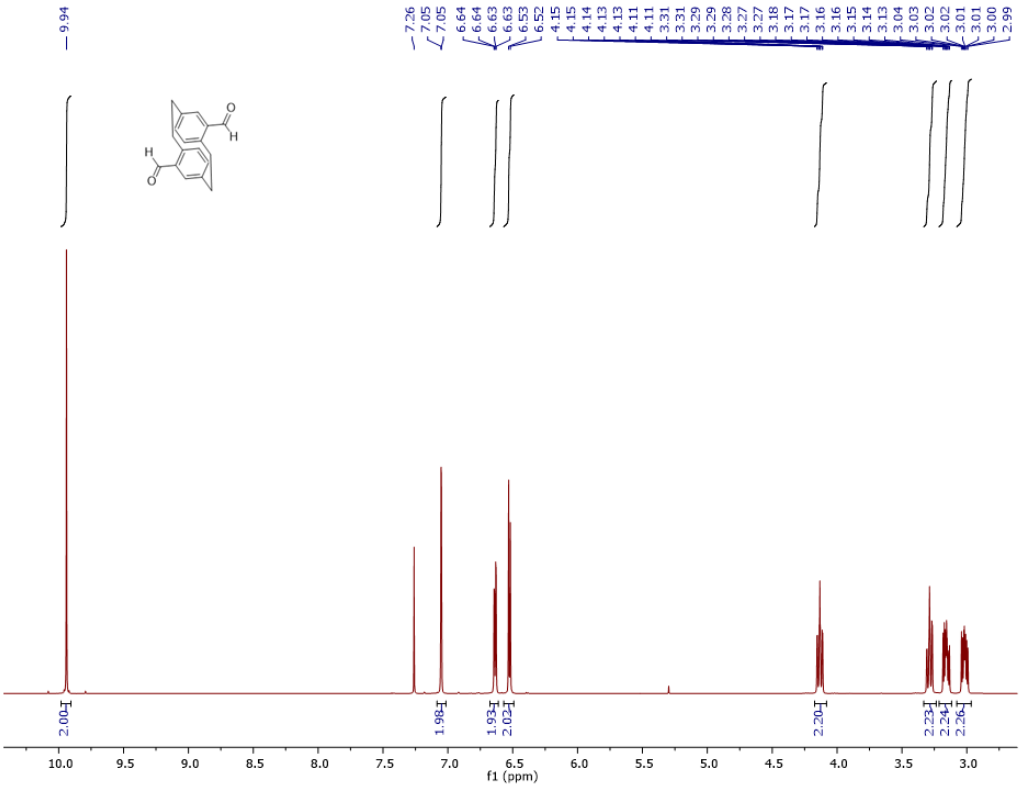

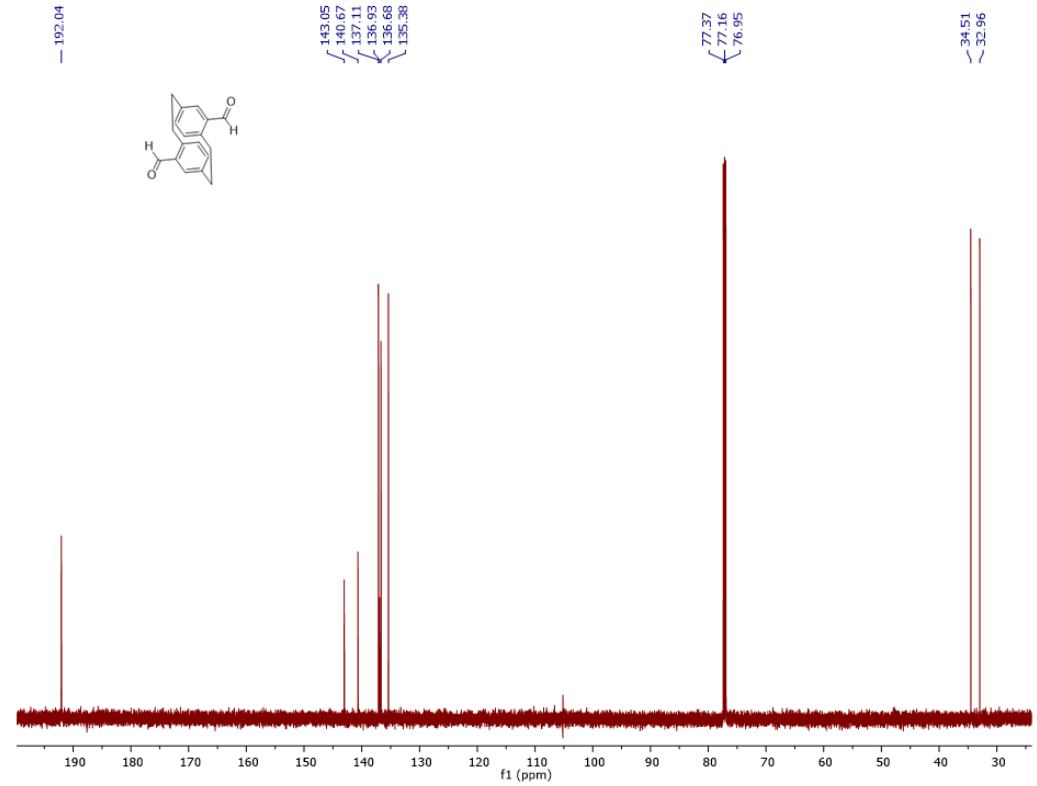

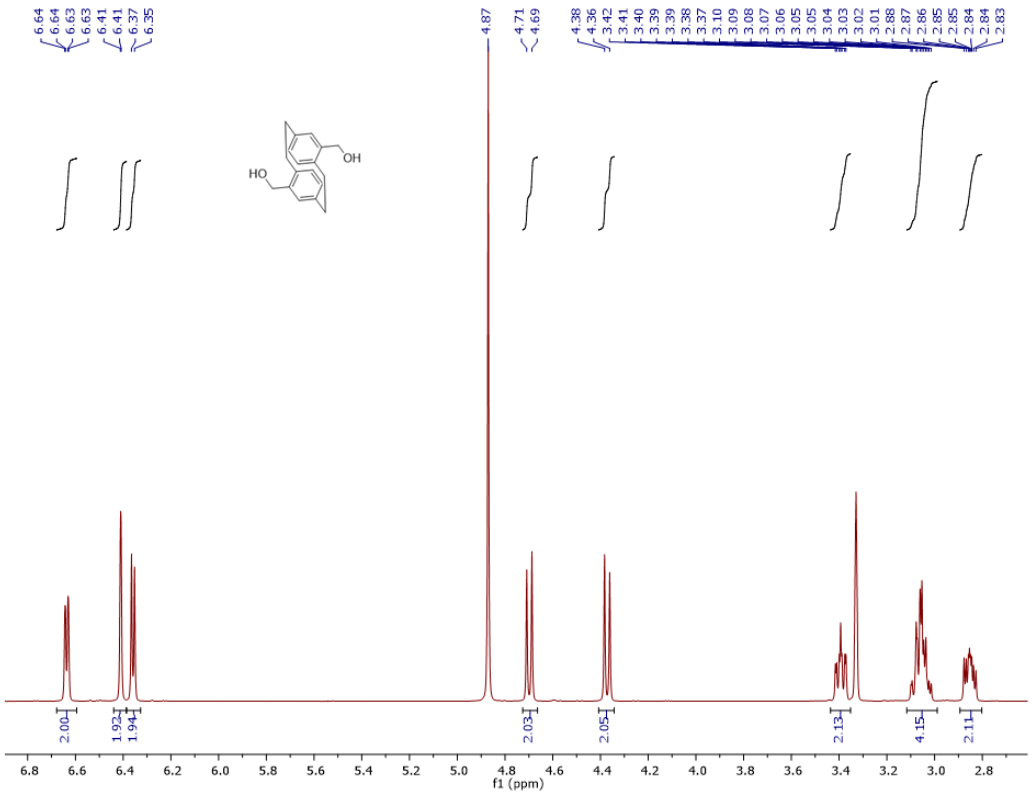
6.64
6.64
6.63
6.63
6.41
6.41
6.37
6.35
4.87
4.71
4.69
4.38
4.36
3.42
3.41
3.40
3.39
3.39
3.38
3.37
3.10
3.09
3.08
3.07
3.06
3.05
3.05
3.04
3.03
3.02
3.01
2.88
2.87
2.86
2.85
2.85
2.84
2.84
2.83
HO
OH
2.00
1.93
1.94
2.03
2.05
2.13
4.15
2.11
6.8 6.6 6.4 6.2 6.0 5.8 5.6 5.4 5.2 5.0 4.8 4.6 4.4 4.2 4.0 3.8 3.6 3.4 3.2 3.0 2.8
f1 (ppm)

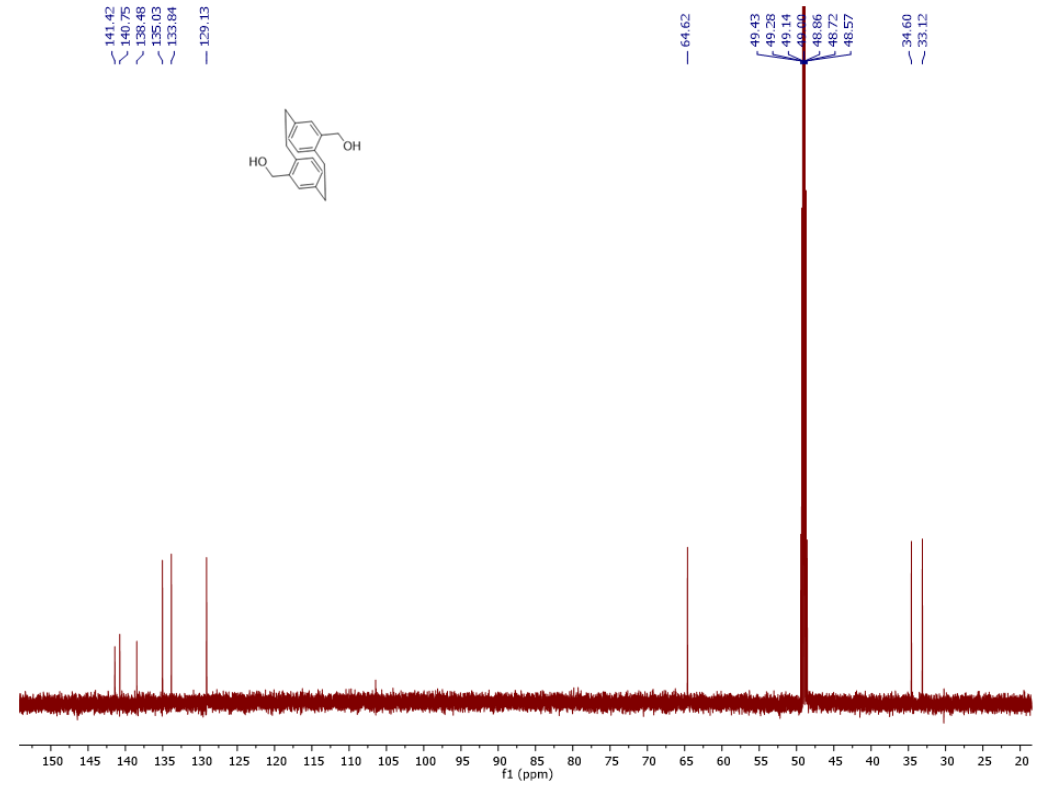
141.42
140.75
138.48
135.03
133.84
129.13
64.62
49.43
49.28
49.14
49.00
48.86
48.72
48.57
34.60
33.12
HO
OH
150 145 140 135 130 125 120 115 110 105 100 95 90 85 80 75 70 65 60 55 50 45 40 35 30 25 20
f1 (ppm)

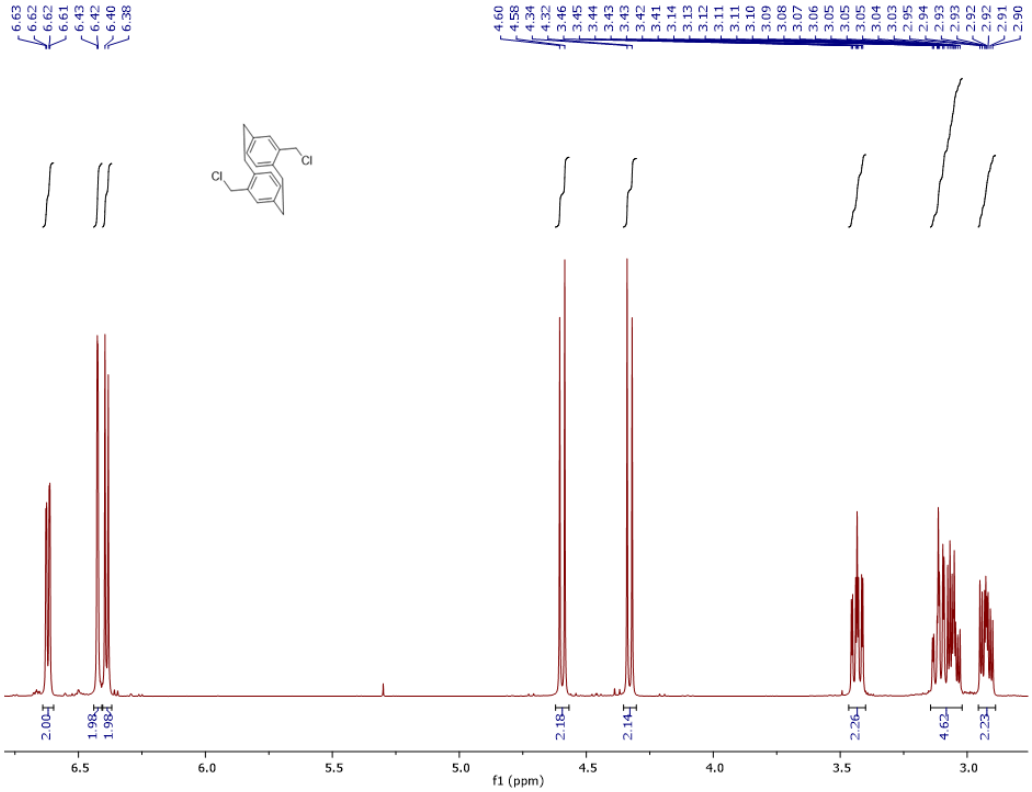
6.63
6.62
6.62
6.61
6.43
6.42
6.40
6.38
4.60
4.58
4.34
4.32
3.46
3.45
3.44
3.43
3.43
3.42
3.41
3.14
3.13
3.12
3.11
3.11
3.10
3.09
3.08
3.07
3.06
3.05
3.05
3.05
3.04
3.03
2.95
2.94
2.93
2.93
2.92
2.92
2.91
2.90
Cl
Cl
2.00
1.98
1.98
2.18
2.14
2.26
4.62
2.23
6.5
6.0
5.5
5.0
4.5
4.0
3.5
3.0
f1 (ppm)

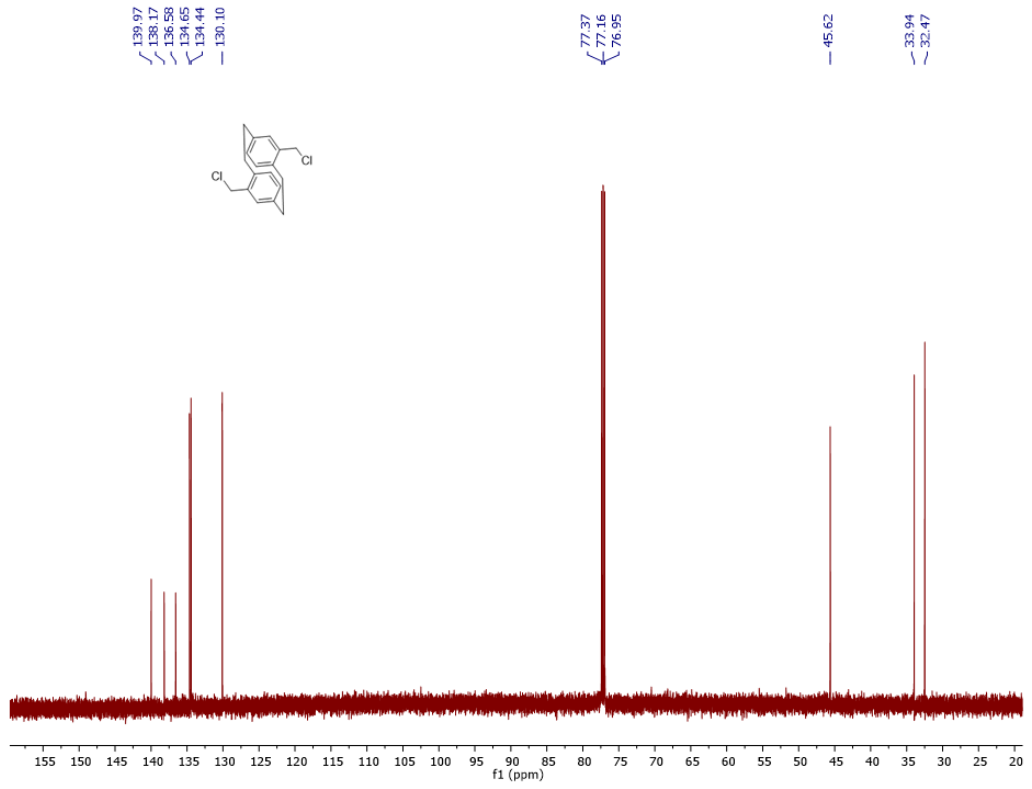
139.97
138.17
136.58
134.65
134.44
130.10
77.37
77.16
76.95
45.62
33.94
32.47
Cl
Cl
155
150
145
140
135
130
125
120
115
110
105
100
95
90
85
80
75
70
65
60
55
50
45
40
35
30
25
20
f1 (ppm)

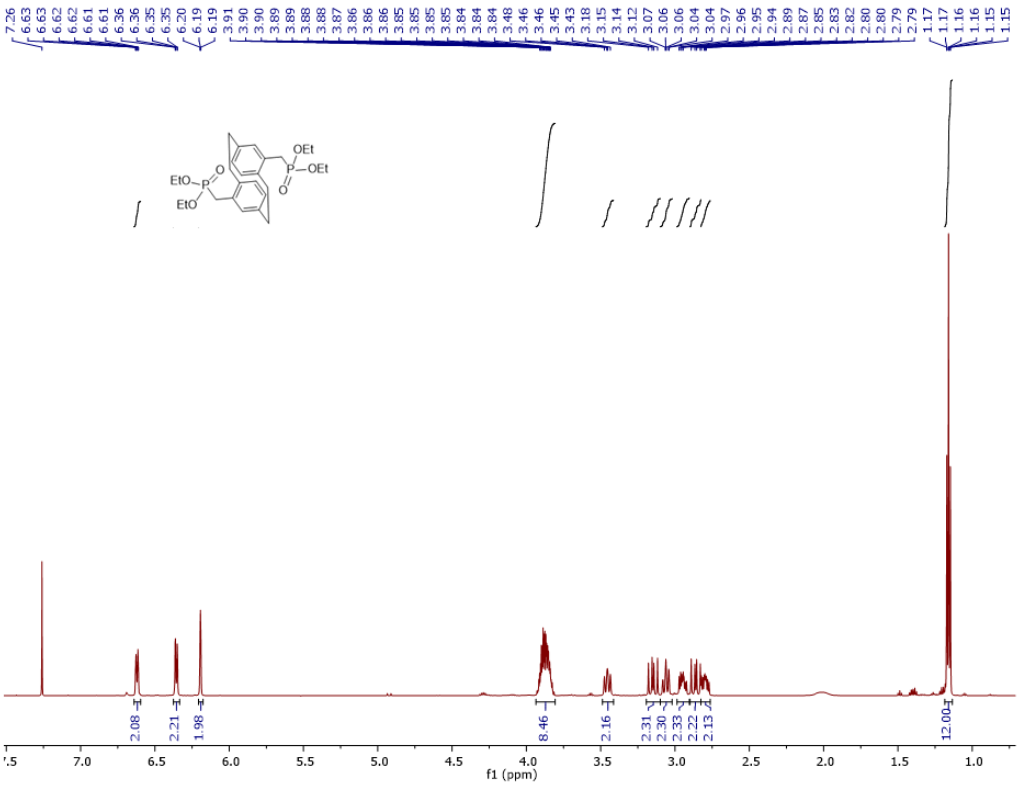
7.26 6.63 6.63 6.62 6.62 6.61 6.61 6.36 6.36 6.35 6.35 6.20 6.19 6.19 3.91 3.90 3.90 3.89 3.89 3.88 3.88 3.87 3.86 3.86 3.86 3.85 3.85 3.85 3.85 3.84 3.84 3.84 3.48 3.46 3.46 3.45 3.43 3.18 3.15 3.14 3.12 3.07 3.06 3.06 3.04 3.04 2.97 2.96 2.95 2.94 2.89 2.87 2.85 2.83 2.82 2.80 2.80 2.79 1.17 1.17 1.16 1.16 1.15 1.15
OEt
EtO
P
O
EtO
P
OEt
O
2.08
2.21
1.98
8.46
2.16
2.31
2.30
2.33
2.22
2.13
12.00
f1 (ppm)

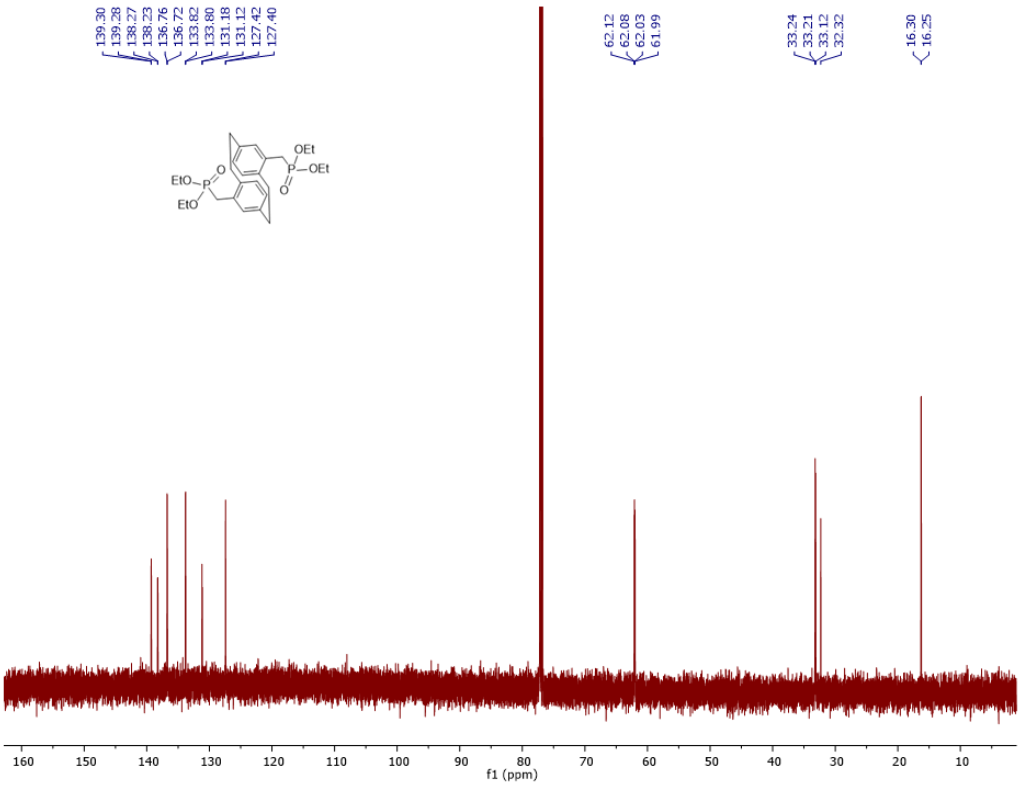
139.30 139.28 138.27 138.23 136.76 136.72 133.82 133.80 131.18 131.12 127.42 127.40
62.12 62.08 62.03 61.99
33.24 33.21 33.12 32.32
16.30 16.25
OEt
EtO
P
O
EtO
P
OEt
O
f1 (ppm)

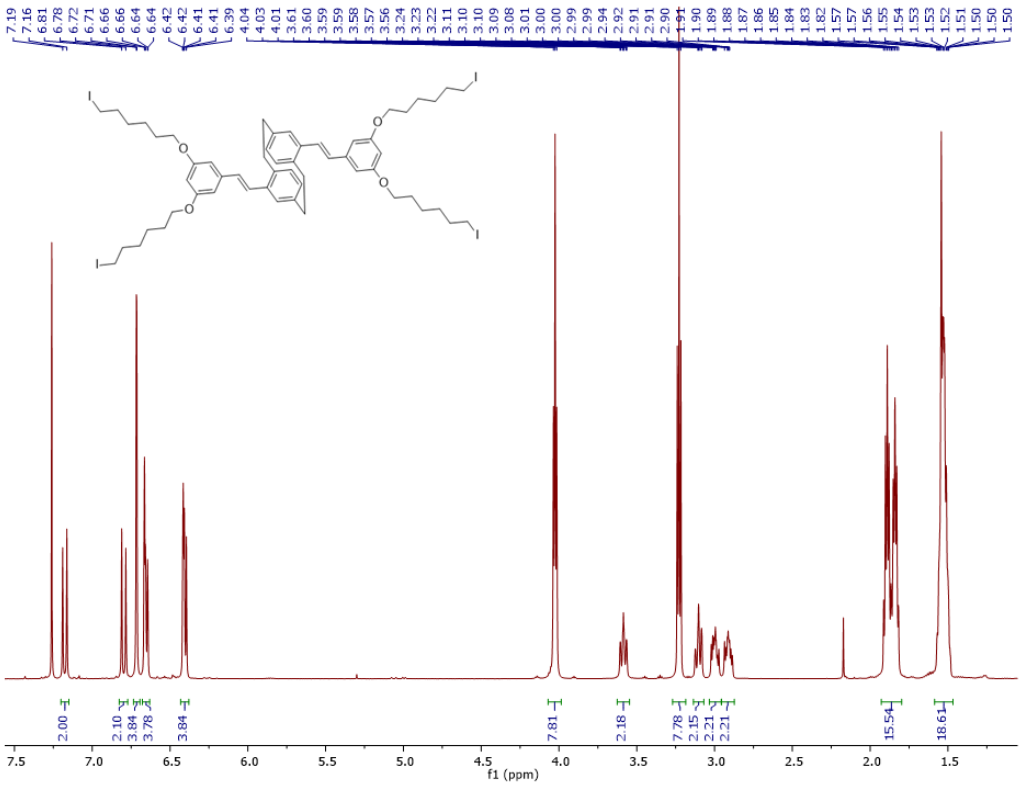
7.19 7.16 6.81 6.78 6.72 6.71 6.66 6.66 6.64 6.64 6.42 6.42 6.41 6.41 6.39 4.04 4.03 4.01 3.61 3.60 3.59 3.59 3.58 3.57 3.56 3.24 3.23 3.22 3.11 3.10 3.10 3.09 3.08 3.01 3.00 3.00 2.99 2.99 2.94 2.92 2.91 2.91 2.90 1.91 1.90 1.89 1.88 1.87 1.86 1.85 1.84 1.83 1.82 1.57 1.57 1.56 1.55 1.54 1.53 1.53 1.52 1.51 1.50 1.50 1.50
2.00 2.10 3.84 3.78 3.84 7.81 2.18 7.78 2.15 2.21 2.21 15.54 18.61
7.5 7.0 6.5 6.0 5.5 5.0 4.5 4.0 3.5 3.0 2.5 2.0 1.5
f1 (ppm)

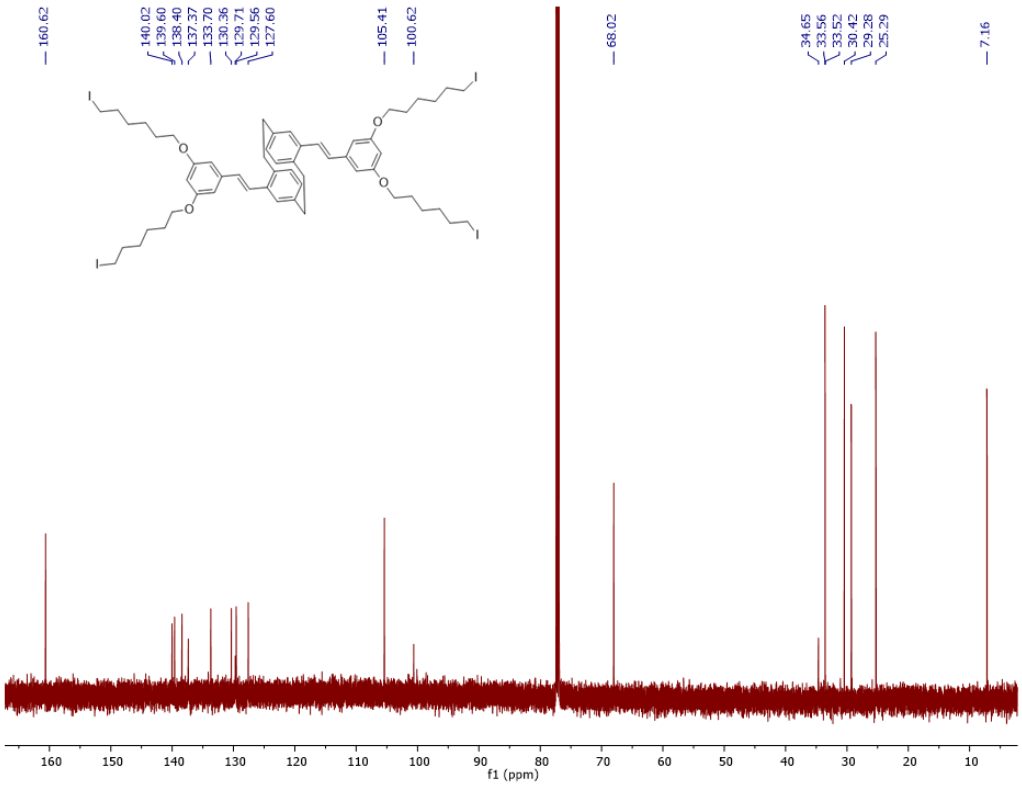
160.62 140.02 139.60 138.40 137.37 133.70 130.36 129.71 129.56 127.60 105.41 100.62 68.02 34.65 33.56 33.52 30.42 29.28 25.29 7.16
160 150 140 130 120 110 100 90 80 70 60 50 40 30 20 10
f1 (ppm)

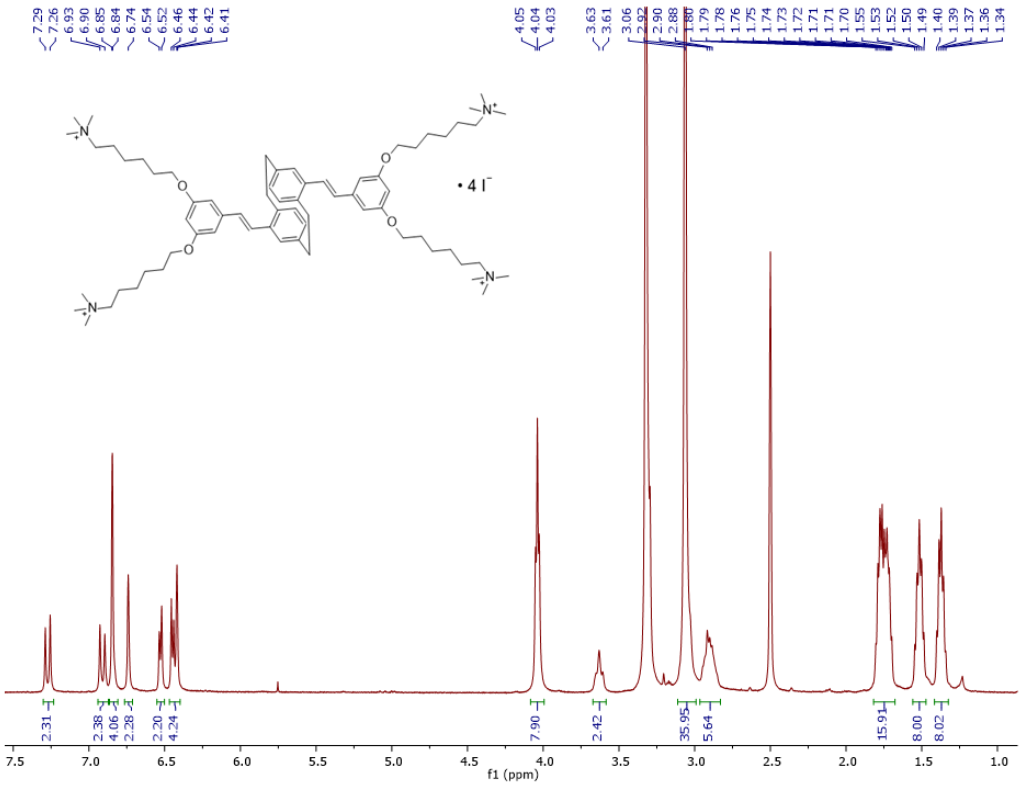
7.29
7.26
6.93
6.90
6.85
6.84
6.74
6.54
6.52
6.46
6.44
6.42
6.41
4.05
4.04
4.03
3.63
3.61
3.06
2.92
2.90
2.88
1.80
1.79
1.78
1.76
1.75
1.74
1.73
1.72
1.71
1.71
1.70
1.55
1.53
1.52
1.50
1.49
1.40
1.39
1.37
1.36
1.34
• 4 I⁻
2.31
2.38
4.06
2.28
2.20
4.24
7.90
2.42
35.95
5.64
15.91
8.00
8.02
7.5
7.0
6.5
6.0
5.5
5.0
4.5
4.0
3.5
3.0
2.5
2.0
1.5
1.0
f1 (ppm)

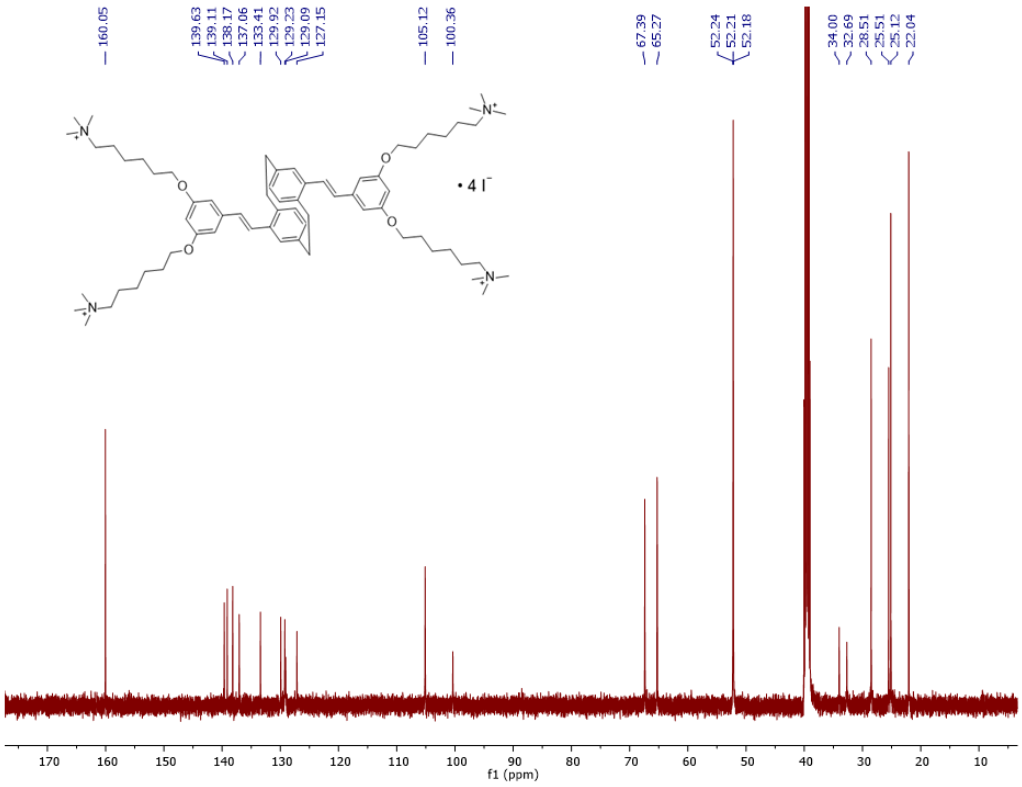
160.05
139.63
139.11
138.17
137.06
133.41
129.92
129.23
129.09
127.15
105.12
100.36
67.39
65.27
52.24
52.21
52.18
34.00
32.69
28.51
25.51
25.12
22.04
• 4 I⁻
170
160
150
140
130
120
110
100
90
80
70
60
50
40
30
20
10
f1 (ppm)

References

1. Wang, Y. *et al.* Membrane Perturbation Activity of Cationic Phenylene Ethynylene Oligomers and Polymers: Selectivity against Model Bacterial and Mammalian Membranes. *Langmuir* **26,** 12509–12514 (2010).
2. Hou, H. *et al.* Conjugated oligoelectrolytes increase power generation in E. Coli Microbial fuel cells. *Adv. Mater.* **25,** 1593–1597 (2013).
3. Yan, H., Catania, C. & Bazan, G. C. Membrane-Intercalating Conjugated Oligoelectrolytes: Impact on Bioelectrochemical Systems. *Adv. Mater.* **27,** 2958–2973 (2015).
4. Thomas, A. W., Catania, C., Garner, L. E. & Bazan, G. C. Pendant ionic groups of conjugated oligoelectrolytes govern their ability to intercalate into microbial membranes. *Chem. Commun.* **51,** 9294–9297 (2015).
5. Hinks, J. *et al.* Modeling cell membrane perturbation by molecules designed for transmembrane electron transfer. *Langmuir* **30,** 2429–2440 (2014).
6. Yan, H. *et al.* Influence of molecular structure on the antimicrobial function of phenylenevinylene conjugated oligoelectrolytes. *Chem. Sci.* **7,** 5714–5722 (2016).
7. Catania, C., Ajo-Franklin, C. M. & Bazan, G. C. Membrane permeabilization by conjugated oligoelectrolytes accelerates whole-cell catalysis. *RSC Adv.* **6,** 100300–100306 (2016).
8. Hinks, J. *et al.* Increased Microbial Butanol Tolerance by Exogenous Membrane Insertion Molecules. *ChemSusChem* **8,** 3718–3726 (2015).
9. Epand, R. F., Pollard, J. E., Wright, J. O., Savage, P. B. & Epand, R. M. Depolarization, bacterial membrane composition, and the antimicrobial action of ceragenins. *Antimicrob. Agents Chemother.* **54,** 3708–3713 (2010).
10. Presečki, A. V., Zelić, B. & Vasić-Rački, D. Comparison of the l-malic acid production by isolated fumarase and fumarase in permeabilized baker's yeast cells. *Enzyme Microb. Technol.* **41,** 605–612 (2007).
11. Garner, L. E. *et al.* Modification of the optoelectronic properties of membranes via insertion of amphiphilic phenylenevinylene oligoelectrolytes. *J. Am. Chem. Soc.* **132,** 10042–10052 (2010).
12. Catania, C., Thomas, A. W. & Bazan, G. C. Tuning cell surface charge in E. coli with conjugated oligoelectrolytes. *Chem. Sci.* **7,** 2023–2029 (2016).
13. Kastowsky, M., Gutberlet, T. & Bradaczek, H. Molecular Modelling of the 3-Dimensional Structure and Conformational Flexibility of Bacterial Lipopolysaccharide. *J Bacteriol* **174,** 4798–4806 (1992).
14. Lu, Q., Wang, J., Faghihnejad, A., Zeng, H. & Liu, Y. Understanding the molecular interactions of lipopolysaccharides during E. coli initial adhesion with a surface forces apparatus. *Soft Matter* **7,** 9366 (2011).
15. Wiegand, I., Hilpert, K. & Hancock, R. E. W. Agar and broth dilution methods to determine the minimal inhibitory concentration (MIC) of antimicrobial substances. *Nat. Protoc.* **3,** 163–175 (2008).
16. Huber, R. E., Kurz, G. & Wallenfels, K. A Quantitation of the Factors Which Affect the Hydrolase and Transgalactosylase Activities of β-Galactosidase (E. coli) on Lactose. *Biochemistry* **15,** 1994–2001 (1976).
17. Mostafa, H. E., Heller, K. J. & Geis, A. Cloning of Escherichia coli lacZ and lacY

Genes and Their Expression in Gluconobacter oxydans and Acetobacter liquefaciens. *Appl. Environ. Microbiol.* **68,** 2619–2623 (2002).
18. de Carvalho, C. C. C. R. Whole cell biocatalysts: essential workers from Nature to the industry. *Microb. Biotechnol.* **10,** 250–263 (2017).
19. Zaknoon, F. *et al.* Antibacterial properties and mode of action of a short acyl-lysyl oligomer. *Antimicrob. Agents Chemother.* **53,** 3422–3429 (2009).
20. Presečki, A. V. & Vasić-Rački, D. Production of L-malic acid by permeabilized cells of commercial Saccharomyces sp. strains. *Biotechnol. Lett.* **27,** 1835–1839 (2005).
21. Berendsen, H. J. C., van der Spoel, D. & van Drunen, R. GROMACS: A message-passing parallel molecular dynamics implementation. *Comput. Phys. Commun.* **91,** 43–56 (1995).
22. Vanommeslaeghe, K. *et al.* CHARMM general force field: A force field for drug-like molecules compatible with the CHARMM all-atom additive biological force fields. *J. Comput. Chem.* **30,** 671–690 (2010).
23. Klauda, J. B. *et al.* Update of the CHARMM All-Atom Additive Force Field for Lipids: Validation on Six Lipid Types. *J. Phys. Chem. B* **114,** 7830–7843 (2010).
24. Jorgensen, W. L., Chandrasekhar, J., Madura, J. D., Impey, R. W. & Klein, M. L. Comparison of simple potential functions for simulating liquid water. *J. Chem. Phys.* **79,** 926–935 (1983).
25. Hess, B., Bekker, H., Berendsen, H. J. C. & Fraaije, J. G. E. M. LINCS: A Linear Constraint Solver for molecular simulations. *J. Comput. Chem.* **18,** 1463–1472 (1997).
26. Miyamoto, S. & Kollman, P. A. SETTLE: An analytical version of the SHAKE and RATTLE algorithm for rigid water models. *J. Comput. Chem.* **13,** 952–962 (1992).
27. Hoover, W. G. Canonical dynamics: Equilibrium phase-space distributions. *Phys. Rev. A* **31,** 1695–1697 (1985).
28. Parrinello, M., Rahman, A. & Parrinello M, R. a. Crystal Structure and Pair Potentials: A Molecular_Dynamics Study. *Phys. Rev. Lett.* **45,** 1196–1199 (1980).
29. Essmann, U. *et al.* A smooth particle mesh Ewald method. *J. Chem. Phys.* **103,** 8577–8593 (1995).